Rydberg Atom Based Electrometry

DR. SETH MEISELMAN
DR. GEOFFREY CRANCH
DR. JANET LOU

Optical Techniques Branch
Optical Sciences Division

DR. SETH RITTENHOUSE
MIDN VANESSA ORTIZ

US Naval Academy
Annapolis, MD

February 13, 2023

REPORT DOCUMENTATION PAGE

Form Approved
OMB No. 0704-0188

1. REPORT DATE *(DD-MM-YYYY)* 13-02-2023	2. REPORT TYPE NRL Memorandum Report	3. DATES COVERED *(From - To)* 2018 – 2022

4. TITLE AND SUBTITLE

Rydberg Atom Based Electrometry

5a. CONTRACT NUMBER

5b. GRANT NUMBER

5c. PROGRAM ELEMENT NUMBER

6. AUTHOR(S)

Seth Meiselman, Geoffrey Cranch, Janet Lou, Seth Rittenhouse*, and Vanessa Ortiz*

5d. PROJECT NUMBER

5e. TASK NUMBER

5f. WORK UNIT NUMBER
1L53

7. PERFORMING ORGANIZATION NAME(S) AND ADDRESS(ES)

Naval Research Laboratory
4555 Overlook Avenue, SW
Washington, DC 20375-5320

8. PERFORMING ORGANIZATION REPORT NUMBER

NRL/5670/MR--2023/1

9. SPONSORING / MONITORING AGENCY NAME(S) AND ADDRESS(ES)

Office of Naval Research
One Liberty Center
875 N. Randolph Street, Suite 1425
Arlington, VA 22203-1995

10. SPONSOR / MONITOR'S ACRONYM(S)

ONR

11. SPONSOR / MONITOR'S REPORT NUMBER(S)

12. DISTRIBUTION / AVAILABILITY STATEMENT

DISTRIBUTION STATEMENT A: Approved for public release; distribution is unlimited.

13. SUPPLEMENTARY NOTES

*US Naval Academy, Dept. of Physics, 121 Blake Rd, Annapolis, MD 21402

14. ABSTRACT

The Rydberg Atom Based Electrometry 6.1 Base Program set out to develop NRL's capability to use highly excited atomic states as a quantum sensor for low frequency (few MHz) electric field measurement. A theoretical framework was derived and new numerical modeling designed to be capable of guiding experiments. A state of the art experimental setup was constructed with future fiber coupling strategies and novel laser frequency locking methods at the forefront. An EIT signal was achieved signaling creation of the $n = 30S$ Rydberg state in room temperature cesium vapor with 2.3 μW of probe power and 2.25 mW of pump power at 852 and 512 nm respectively.

15. SUBJECT TERMS

Rydberg	Electromagnetically induced transparency	EIT	Electrometry
Electric field sensing	Atomic Sensing	Quantum sensing	Quantum sensor

16. SECURITY CLASSIFICATION OF:

a. REPORT U	b. ABSTRACT U	c. THIS PAGE U	17. LIMITATION OF ABSTRACT U	18. NUMBER OF PAGES 16	19a. NAME OF RESPONSIBLE PERSON Seth J. Meiselman
					19b. TELEPHONE NUMBER *(include area code)* (202) 404-5432

Standard Form 298 (Rev. 8-98)
Prescribed by ANSI Std. Z39.18

This page intentionally left blank.

CONTENTS

FIGURES

TABLES

This page intentionally left blank

EXECUTIVE SUMMARY

The Rydberg Atom Based Electrometry 6.1 Base Program set out to develop NRL's capability to use highly excited atomic states as a quantum sensor for low frequency (few MHz) electric field measurement. A theoretical framework was derived and new numerical modeling designed to be capable of guiding experiments. A state of the art experimental setup was constructed with future fiber coupling strategies and novel laser frequency locking methods at the forefront. An EIT signal was achieved signaling creation of the n = 30S Rydberg state in room temperature cesium vapor with 2.3 μW of probe power and 2.25 mW of pump power at 852 and 512 nm respectively.

This page intentionally left blank

RYDBERG ATOM BASED ELECTROMETRY

1. INTRODUCTION

The primary objective of the Rydberg Atom Based Electrometry 6.1 Base Program is to demonstrate measurement of low frequency electric fields through AC and DC Stark shifts in a highly excited Rydberg state of cesium. This kind of sensor could lead to a new generation of contactless, all-optical, point-like electric field sensors with resolution limited by fundamental quantum noise. The development of Rydberg atom based sensors should have a broad impact on applications requiring high precision electric field measurements in both atmospheric and underwater environments.
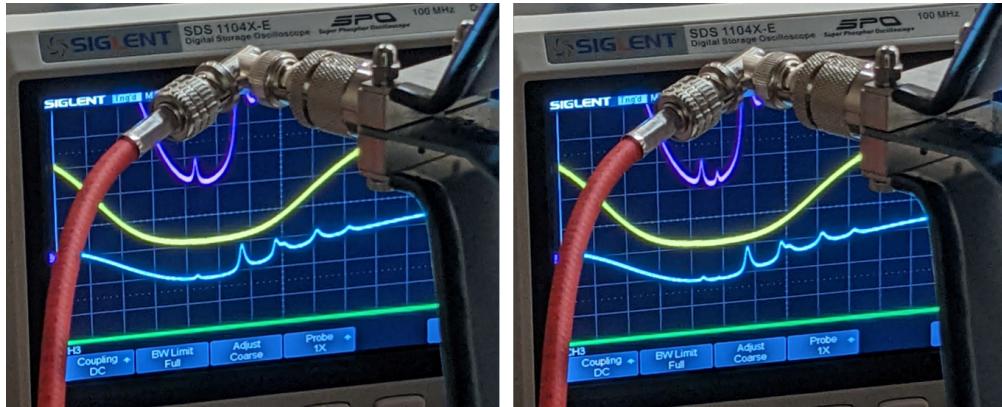
Fig. 1—Left: Display of oscilloscope showing saturated absorption spectroscopy signals when no 510 nm beam is passing through the setup. Right: Display of oscilloscope showing saturated absorption spectroscopy signals when the 510 nm beam is passing through the setup. The additional peak, clearly seen in the pink trace of the right photo is the EIT window, verifying excitement to the n = 30 S state in cesium vapor, at room temperature with no additional RF field present.

Fundamentals of Rydberg systems and capabilities can be found in [1–4] for background Rydberg calculations, electromagnetically induced transparency (EIT, see Fig. 1) and manipulation of signal dependency on DC field. A limitation to our work is applications at room temperature, or more accurately at ambient temperature. This would necessitate understanding the influence of black body radiation interactions with the Rydberg state [5–8].

Table 1 lists references that exhibit using atoms for measuring at various frequencies. Our interest in using Rydberg atoms to conduct RF or microwave sensing [9–12] stems from these quantum systems being capable of measuring electric field strength as a fundamental, calibration free measurement, traceable to frequency standards [13]. We notice that most of the current research efforts for using atoms to measure RF fields fall into two categories: 3 MHz and below (MF and lower bands) and 1 GHz and above (UHF or SHF and higher bands).

Reference	E	H	Frequency		Source:Signal
[14]	X		36-37	GHz	Horn: 1 kHz AM
[15]	X		19.6	GHz	Horns with Δf=1 kHz to 2.5 MHz
					(10 MHz limit)
[16]	X		19.6	GHz	Horns with Δf=90 kHz
[17]	X		16.98	GHz	Horn: AM 440 Hz-1.76 kHz
					(60 kHz bandwidth)
[18]		X	99	kHz	Coils (in shield)
[19]		X	DC-1	kHz	Speaker coil (outside shield):
					BPSK up to 1 kHz
[20]		X	< 50	kHz	Coils (in shield): 1 kHz PM
					(1.5 kHz bandwidth)
[21]		X	6.835	GHz	Loop (3 mm D): 400 Hz FM with 500 Hz mod depth
[22]		X	2.87	GHz	Helix: AM
					(200 MHz bandwidth)
[23]		X	16-100	kHz	Square coil (35 mm side): LIA frequency limited to 100 kHz
					(0.13 Hz MOT loading time)
[24]		X	e.g. 10	kHz	Coils (in shield):
					AC frequency = Larmor frequency of DC field
[25]		X	0.5-1.31	MHz	Coil (with zero DC):
					0.6 us pulses
[26]		X	16.6	kHz	Test subject (in zero DC):
					(140 Hz bandwidth)
[27]		X	1-100	Hz	Coils (in shield)
[28]		X	9.2	GHz	Waveguide
[29]		X	9.2	GHz	Microwave cavity
[30]		X	2.3-26.4	GHz	Microwave device
[31]		X	5.25	kHz	Coils (in shield)
[32]		X	1.3	MHz	RF coil (for NMR)
[33]		X	62	kHz	RF coil (for NMR)
[34]		X	< 400	kHz	Coils

Table 1—List of literature references (not to be considered exhaustive, but representative) with sensing modality and frequency (range) being sensed.

See Appendix A of [35] for transition frequencies calculated from the ARC software package [36], as this should help illuminate why Rydberg atoms in general can claim to measure fields at such vastly different frequencies. The difference between neighboring Rydberg energy states that starts widely spaced, can shrink to a few MHz near the n = 150-180 S and D states in cesium alone (different alkali species have different energy spacings).

2. THEORETICAL FRAMEWORK

In the literature, a common practice is to use a three-field interaction scheme (see [13] as an example) where the RF field couples two Rydberg states. In a long-view consideration of this scheme, one main issue arises: if the RF field is far detuned from any transition to be coupled, the interaction breaks down and no observation of the RF field occurs. If instead a method was to allow for any RF field as a perturbation to a preexisting two-field inteaction, seemingly any RF frequency should be able to be observed. This is precisely what is described in [12] with Floquet analysis.

As partially described in [35], we are looking to solve the following time dependent Schrödinger equation

$$\hat{H}|\Psi(t)\rangle \;=\; i\hbar\frac{\partial}{\partial t}|\Psi(t)\rangle \tag{1}$$

$$\hat{H} \;=\; \hat{H}_{Ryd} + \vec{d}\cdot\vec{F}(t) \tag{2}$$

where $\hat{H}_{Ryd}$ is the Hamiltonian for the bare Rydberg system, $\vec{d}$ is the atomic dipole moment and $\vec{F}(t)$ is a time varying electric field. We are specifcally going to take that the electric field is an RF field with a DC offset, i.e. $\vec{F}(t) = \vec{F}_0 + \vec{F}_1(t)$ with $\vec{F}_1(t) = \vec{F}_1\cos(\omega t)$. We will start by assuming that the oscillation in the field is slow enough that we can use the wave function to be the ns-wave dominated DC Stark state. In other words

$$\left(\hat{H}_{Ryd} + \vec{d}\cdot\vec{F}(t)\right)|\Psi_{DC}\rangle \;=\; E_{DC}|\Psi_{DC}\rangle, \tag{3}$$

notice that here the Start shift energy E_{DC} is dependent only on the magnitude of the electric field. We can expand the DC Stark wave function in Rydberg states ψ_k as

$$|\Psi_{DC}\rangle \;=\; \sum_k |\psi_k\rangle \tag{4}$$

where we will assume ψ_0 is the nS Rydberg state that we are exciting to. Inserting this wave function above gives

$$E_{DC}\left(\left|\hat{F}_0 + \vec{F}_{RF}(t)\right|\right)|\Psi(t)\rangle \;=\; i\hbar\frac{\partial}{\partial t}|\Psi(t)\rangle. \tag{5}$$

In truth, because we have a time varying field, the DC wave function expansion coefficients acquire a time dependence as well. However, we are going to assume that the nS state amplitude is very weakly time dependent and can be approximated as that given by the DC field offset alone, i.e. $a_0(F(t)) = a_0(F_0) = a_0$. Thus we will absorb all of the time dependence into a separate function, i.e. $|\Psi(t)\rangle = T(t)|\Psi_{DC}(F_0)\rangle$.

The two-photon excitation will only pick out the s-wave states, and the sates far away from the nS state of interest will have a vanishingly small contribution to the final Rabi frequency of the $6P - nS$ transistion meaning that we only care about the behavior of the ψ_0 state in the above scenario. Projecting onto this state yields

$$E_{DC}\left(\left|\hat{F}_0 + \vec{F}_{RF}(t)\right|\right)T(t) \quad = \quad i\hbar\frac{\partial}{\partial t}T(t) \tag{6}$$

where we have canceled the factor of a_0 that appeared on either side.

Because the field varies harmonically with frequency ω, we can make the Floquet assumption here and the time behavior is a Fourier series with Fourier coefficients β_l:

$$T(t) \quad = \quad e^{-iE_0t/\hbar}\sum_{l=-\infty}^{\infty}\beta_l e^{-il\omega}, \tag{7}$$

where E_0 will be the energy of the $l = 0$ states. We will also assume that the RF field is very weak and we are in the linear regime of the stark shift, i.e. $E_{DC}\left(\left|\hat{F}_0 + \vec{F}_{RF}(t)\right|\right) \approx E_{DC}(F_0) + \gamma\frac{F_{RF}}{2}\left(e^{i\omega t} + e^{-i\omega t}\right)$. Notice here that F_{RF} is not just the magnitude of the RF field, it is the linear term in the expansion of the magnitude of the total electric field, i.e. $\left|\vec{F}_0 + \vec{F}_{RF}(t)\right| \approx F_0 + F_{RF}\cos(\omega t)$. Inserting all of this gives

$$\sum_{l=-\infty}^{\infty}\left[E_{DC}\beta_l + \gamma\frac{F_{RF}}{2}(\beta_{l+1} + \beta_{l-1})\right]e^{-il\omega} \quad = \quad \sum_{l=-\infty}^{\infty}(\Delta E + l\hbar\omega)\beta_l e^{il\omega} \tag{8}$$

where $\Delta E = E_0 - E_{DC}(F_0)$ and we have canceled out a common factor of $e^{-iE_0t/\hbar}$. If we now project onto the individual Fourier components, we get a difference equation for the expansions coefficients β_l:

$$E_{DC}\beta_l + \frac{F_{RF}}{2}(\beta_{l+1} + \beta_{l-1}) \quad = \quad (\Delta E + l\hbar\omega)\beta_l. \tag{9}$$

The solution to this difference equation is actually Bessel functions

$$\beta_l \quad = \quad c_1 J_{(\Delta E/\hbar\omega + l)}\left(\frac{\gamma F_{RF}}{\hbar\omega}\right) + c_2 Y_{(\Delta E/\hbar\omega + l)}\left(\frac{\gamma F_{RF}}{\hbar\omega}\right) \tag{10}$$

where $J_\nu(z)$ and $Y_\nu(z)$ are Bessel functions of the first and second kind respectively. Remembering that β_l is the lth Fourier component of the state with energy E_0 we can assume that there is no contribution from the infinite frequency Fourier components, i.e. $\lim_{l\to\pm\infty}\beta_l = 0$. We now will assume that $\gamma F_{RF} << \hbar\omega$ meaning that as $l \to \infty$ we must have that $c_2 = 0$. Finally to enforce that $\lim_{l\to\pm\infty}\beta_l = 0$ we must then have that the Bessel function is of integer order, i.e. $E_0 = E_{DC}(F_0) + n\hbar\omega$ finally giving

$$\beta_l^{(n)} \quad \propto \quad J_{n+l}\left(\frac{\gamma F_{RF}}{\hbar\omega}\right). \tag{11}$$

This then gives the Fourier amplitude of the *lth* Fourier component in the *nth* side band. The $l = 0$ component is the one that contributes to the $6P - nS$ transition Rabi-frequency. We then finally have that the Rabi frequency of the nth side band state at energy $E_{DC}(F_0) + n\hbar\omega$ is

$$\beta_0^{(n)} \quad \propto \quad J_n\left(\frac{\gamma F_{RF}}{\hbar\omega}\right).$$
(12)

Figures produced in both Appendix A, Fig. A1 and in [35] come from a Mathematica notebook script which can be made available upon request.

3. EXPERIMENTAL SETUP
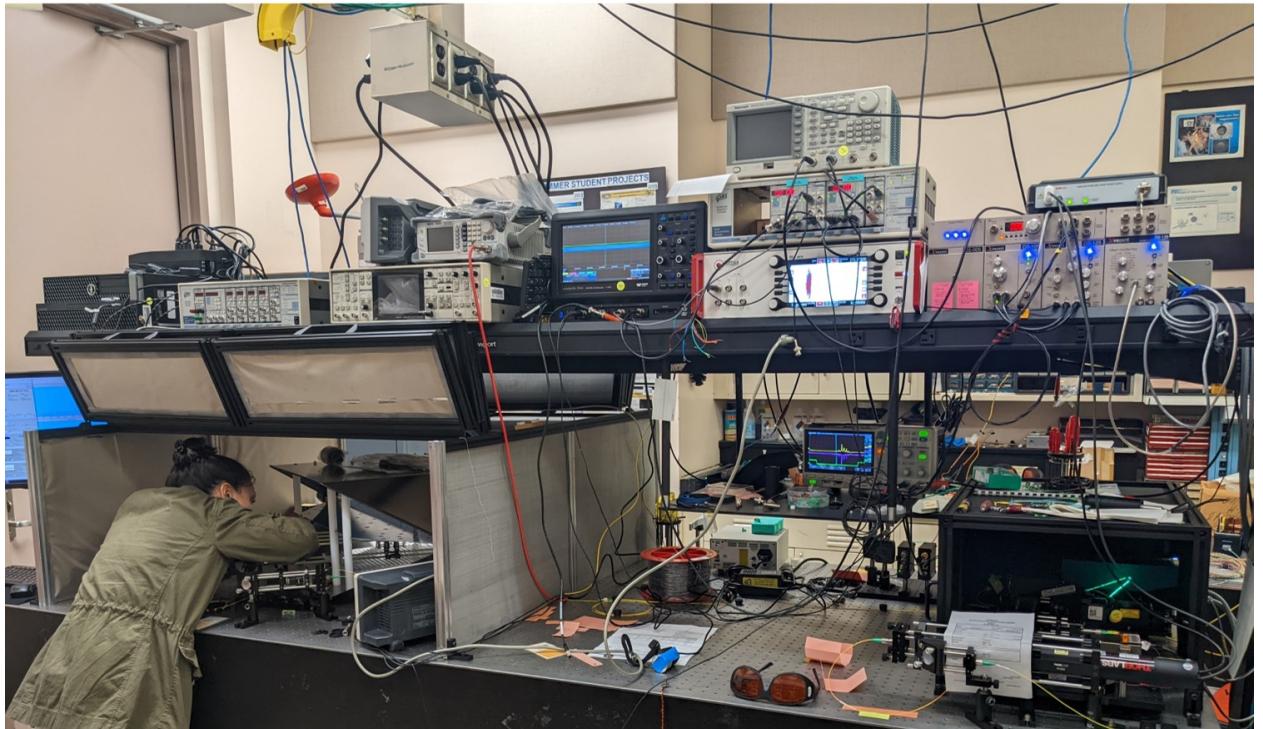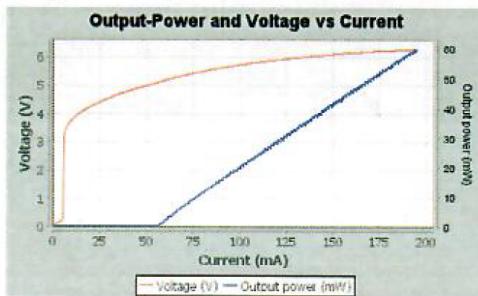
Fig. 2—Experimental setup in the laboratory. Shown is MIDN Ortiz adjusting the focal the
852 nm probe beam to be centered with the focus of the 510 nm beam. This work was aided
by calculations in Appendix B.

The TOPTICA DLC PRO laser system used for our Rydberg excitation field is designed for coarse tunability of a wide range, 508.48 to 512.2 nm, see Fig. 3. This corresponds to frequencies of 585.303 to 589.585 THz, which may be compared to excitations in Appendix A of [35]. To properly address the n = 30S state in cesium we require the laser to operate outside its designed specifications at 584.9312 THz, or 512.526 nm. Operating at this wavelength allows us to see the EIT window shown in Fig. 1. One consequence of this choice is a reduction in operational power output from the laser head, another is sensitivity to destabilization effects. To recover stable laser operation we developed a fiber based stabilization and measurement strategy outlined in Appendix B of [35].

07 Free Running Laser Diode

Wavelength:	511.04 nm	**Temperature:**	19.9 °C
Lasing Threshold:	58 mA	**Slope Efficiency:**	0.424 W/A
Maximum Power:	59.8 mW		
Maximum Current:	195 mA		

Output Power vs. Current Characteristics: **Optical Spectrum (RBW = 0.05 nm):**
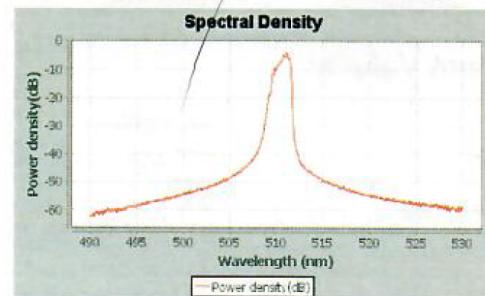
Fig. 3—The TOPTICA DLC Pro laser is designed for a 510 nm wavelength. The external
cavity diode laser is coarsely tunable over a 509-512 nm range.

A Falco Systems WMA-200 low-noise, high-voltage amplifier provides a x19 amplification of the input voltage at 1 A to a maximum output of ±175 V at 2 A. This is driven by a HP 3314A function generator with square wave output at 200 Hz. For our purposes with the stretching the MZI arm, 1.52mV is enough to drive the fiber stretcher through the amplifier to get sufficient change in path imbalance. The fiber stretcher described in [35], uses as Steiner & Martins, Inc. piezo stack actuator with 3 μF ± 20%. At 150 V, 200 Hz, this yields a 40mum ± 10% in linear stretch, which then doubles for a single loop. The fiber stretcher is tightly wound with 125.5 turns, giving a nominal 10.04 mm of change in path imbalance.

Following the derivation in the appendix of [35], a long term drift of the HeNe laser resolution of 3 MHz and a measurement of the fringe counting near 0.0005/fringe, $d\lambda = 1.2 \times 10^{-11}$mm or $d\nu = 13.84$ MHz. Refining the fringe measurement to by a factor of 5 translates into reduction of $d\nu = 5.75$ MHz. The static path imbalance of the MZI was respliced to less than one centimeter. This was to remove laser frequency noise. This interferometric measurement scheme allows us to measure the wavelength of the 510 nm light better than the WS6-200 wavemeter from High Finesse we otherwise have available in the lab.

The script for locking the 510 nm laser to the HeNe (at 633 nm) through the fiber MZI:

1. stabilize MZI temperature and motion to lock

2. apply sine wave to PZT

3. look for interference on differential output

4. adjust polarization control of HeNe input to maximize interference

5. disconnect sine source

6. turn on PID with low gain

7. adjust gain aiming differential out towards zero

8. operate with PID τ as high as possible

9. repeat for 510 nm

Successful locking of the 510 to the HeNe was made with the HeNe PID at 1.0E3, and 510 PID at 0.1E4 using SRS PID modules. The PID settings were P and I focused, D coefficients were set to unity.
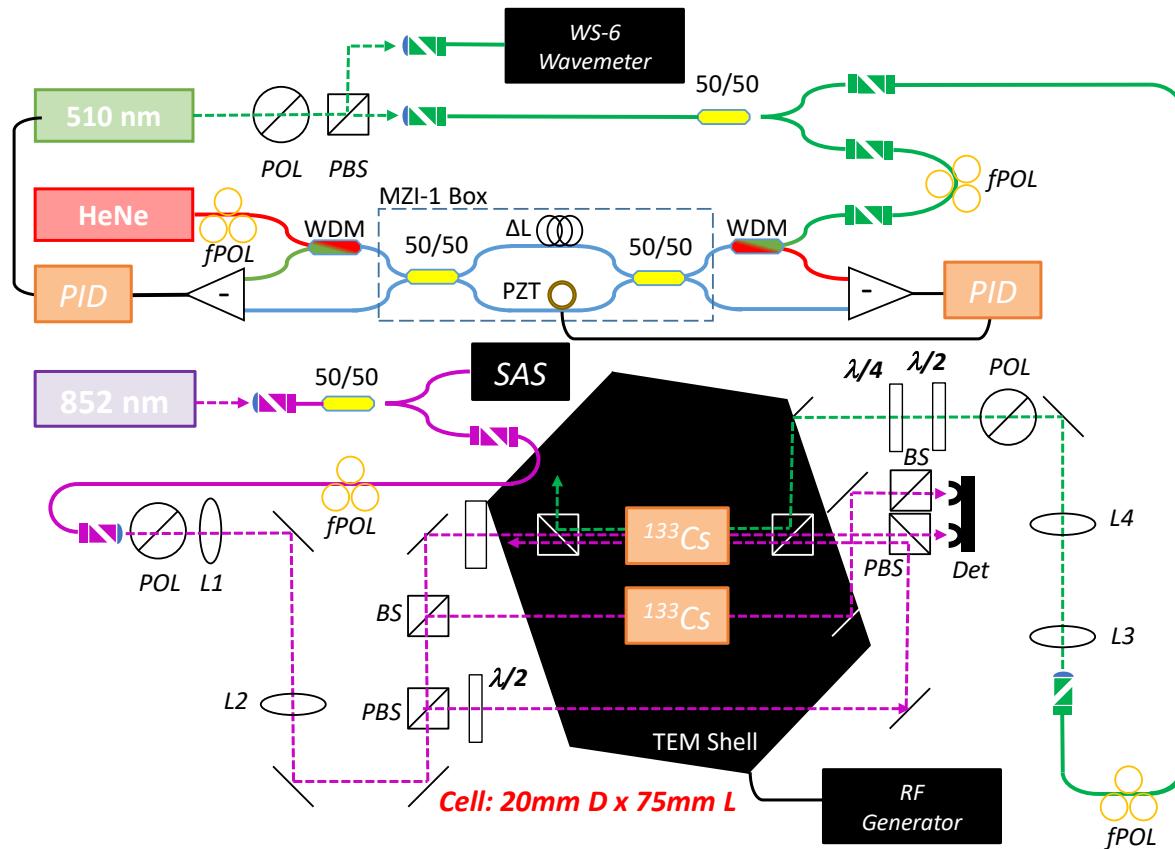
Fig. 4—Rydberg Atom Based Electrometry experimental setup. POL polarizer, fPOL fiber polarization controller, PBS polarizing beam splitter, BS beam splitter, WDM wavelength demultiplexer, MZI Mach-Zender interferometer, PZT piezoelectric transducer, 50/50 fiber coupled beam splitter, ΔL fiber delay length, $\lambda/2$ half waveplate, $\lambda/4$ quarter waveplate, LP/DF longpass dichroic filter, L1-L4 lens, Det detector, SAS Saturated Absorption Spectroscopy module. The 510 nm laser is frequency locked to the HeNe for measurement stability after being carefully tuned to be resonant with the Rydberg state of interest. The 852 nm laser is allowed to be unlocked for initial viewing of the EIT window, and can be locked for signal increase. TEM Shell is a compliance cell testing device, used here to deliver the RF field.

Using the experimental setup we could take saturated absorption spectroscopy-like signals, see Fig. 5 and Fig. 6 that allow us to compare numerical modeling of the hyperfine ground states to what exists in the vapor cell. The numerical model and outputs can be found in Appendix C.
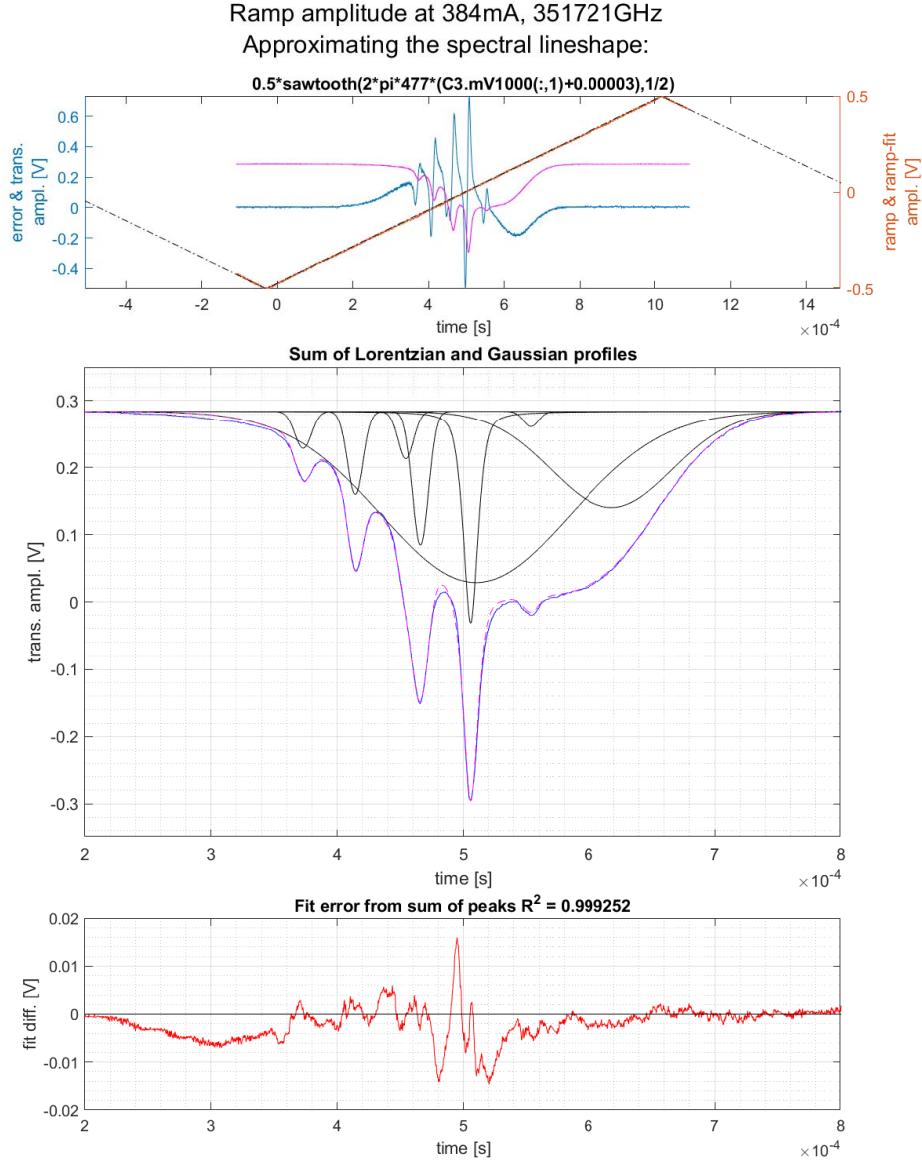
Fig. 5—The Vescent D2-100-DBR Distributed Bragg Reflector laser is designed for a 852 nm wavelength, exciting the D2 transition in atomic cesium. The laser can be finely swept over a narrow range (less than 1 GHz), or can be coarsely tuned over a 9.2 GHz to inspect both the F=3 to F'=(2,3,4) and F=4 to F'=(3,4,5) transitions. See Fig. D2 for more details. Here we have fit the hyperfine transitions, including crossover peaks, from the F=3 state with Lorentzian lineshapes, and Gaussian profiles for the thermal broadened fine structure state. The Lorentzian lineshapes relate to the relaxation rate of the ground state excitation, see Fig. C3.
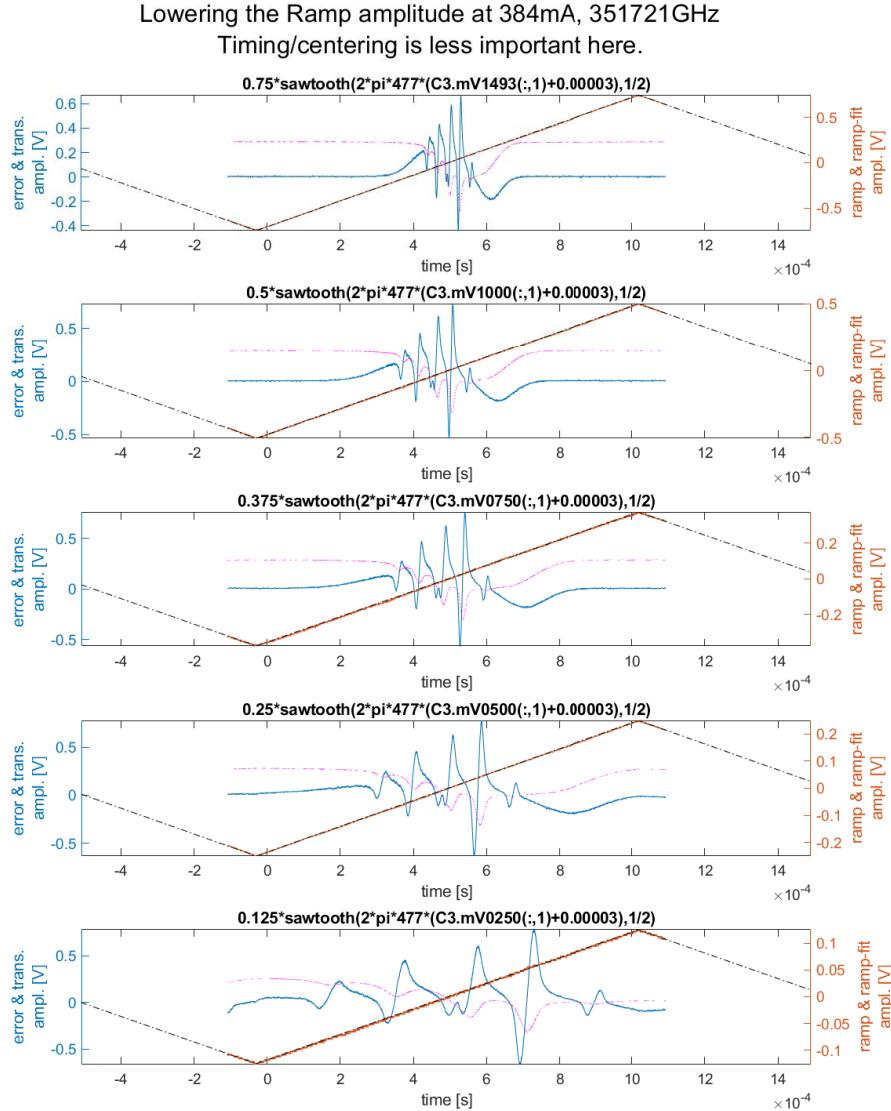
Fig. 6—The Vescent D2-100-DBR laser voltage ramp is adjusted to control the scan amplitude. The laser can be finely swept over a single hyperfine transition (less than 10 MHz). The variable scan amplitude translates into a variable frequency spacing over the approximate 500 Hz repetition rate of the triangle waveform. Furthermore, though not obvious here, the influence of the ramp function is not symmetric, the 'beginning' of a ramp has a different frequency spacing than the 'end', occurring for both positive and negative ramp slopes. This detail caused initial ambiguity in measuring the Lorentzian lineshape widths show in Fig. 5.

The TEM compliance cell shown in Fig. 2 and outlined as in Fig. 4 was chosen to apply the low-frequency fields of interest since an RF horn for 10-100 MHz would be too large for the laboratory setting. Driven by a Rigol DSG815 RF signal source capable of 9 kHz-1.5 GHz output, the Tekbox TBTC3 TEM cell provides a large enough working volume between the outer shell and septum to fit our vapor cell (20 mm diam. by 75 mm long) and common opto-mechanics, and operates over the frequency region of interest.

A custom Faraday cage was constructed surrounding the TEM cell and optical setup. This consisted of an extruded aluminum frame, polycarbinate sheeting for wall stability, two layers of TitanRF Faraday fabric, and a layer of fine mesh steel cloth. The double layer of TitanRF fabric provides attenuation of 90 dB or more for frequencies less than 5 GHz. The additional fine mesh steel cloth ensures stronger attenuation at lower frequencies, towards 1 kHz. This is primarily focused on background removal of common laboratory electronic noise (including WiFi, etc.).

4.   FUTURE PROGRAM GOALS

Previous investigations into multipass techniques were focused on highly precise polarization alignment for carefully controlled, polarization dependent interactions [37]. It may be possible to leverage simple multipass methods to increase signal strength if further development can confirm looser polarization maintaining concerns.

The Floquet simulations need experimental observables to accurately describe the physics of the EIT response. These include the lifetimes or state widths, transition amplitudes or strengths, and the precise laser powers and focal spot size or intensities to yield the dephasing rates used in the simulation.

The current numerical modeling approach base on Floquet analysis requires huge sets of states for individual frequencies being modeled. In practice, this becomes exorbitant at four 'single' frequencies. Investigation into a generalized frequency function $f(\omega)$ to allow an arbitrary environment and radio signal interaction would be widely beneficial. This change may require a new framework from the existing Floquet analysis being used, further consideration would tie in well to a follow on 6.1 Base Program.

REFERENCES

1.   M. L. Zimmerman, M. G. Littman, M. M. Kash, and D. Kleppner, "Stark structure of the Rydberg states of alkali-metal atoms," *Phys. Rev. A* **20**, 2251–2275 (Dec 1979), doi:10.1103/PhysRevA.20.2251. URL `https://link.aps.org/doi/10.1103/PhysRevA.20.2251`.

2.   T. F. Gallagher, *Rydberg Atoms*, 1st ed. (Cambridge University Press, 1994).

3.   A. K. Mohapatra, T. R. Jackson, and C. Adams, "Coherent Optical Detection of Highly Excited Rydberg States Using Electormagnetically Induced Transparency," *Phys. Rev. Lett.* **98**(113003) (2007), doi:10.1103/PhysRevLett.98.113003. URL `https://journals.aps.org/prl/abstract/10.1103/PhysRevLett.98.113003`.

4.   L. A. Jones, J. D. Carter, and J. D. D. Martin, "Rydberg atoms with a reduced sensitivity to dc and low-frequency electric fields," *Phys. Rev. A* **87**, 023423 (Feb 2013), doi:10.1103/PhysRevA.87.023423. URL `https://link.aps.org/doi/10.1103/PhysRevA.87.023423`.

5. S. Kumar, H. Fan, H. Kübler, A. J. Jahangiri, and J. P. Shaffer, "Rydberg-atom based radio-frequency electrometry using frequency modulation spectroscopy in room temperature vapor cells," *Opt. Express* **25**(8), 8625–8637 (Apr 2017), doi:10.1364/OE.25.008625. URL `http://www.opticsexpress.org/abstract.cfm?URI=oe-25-8-8625`.

6. L. Zhang, Y. Jia, M. Jing, L. Guo, Z. Zhang, L. Xiao, and S. Jia, "Detuning radio-frequency electrometry using Rydberg atomcs in a room-temperature vapor cell," *Laser Phys.* **29**, 035701 (2019). URL `https://iopscience.iop.org/article/10.1088/1555-6611/aaffcb`.

7. J. W. Farley and W. H. Wing, "Accurate calculation of dynamic Stark shifts and depopulation rates of Rydberg energy levels induced by blackbody radiation. Hydrogen, helium, and alkali-metal atoms," *Phys. Rev. A* **23**, 2397–2424 (May 1981), doi:10.1103/PhysRevA.23.2397. URL `https://doi.org/10.1103/PhysRevA.23.2397`.

8. D. B. Branden, T. Juhasz, T. Mahlokozera, C. Vesa, R. O. Wilson, M. Zheng, A. Kortyna, and D. Tate, "Radiative lifetime measurements of rubidium Rydberg states," *J. Phys. B: At. Mol. Opt. Phys.* **43**(015002) (2010). URL `https://iopscience.iop.org/article/10.1088/0953-4075/43/1/015002/meta`.

9. J. A. Sedlacek, A. Schwettmann, H. Kübler, R. Löw, T. Pfau, and J. P. Shaffer, "Microwave electrometry with Rydberg atoms in a vapour cell using bright atomic resonances," *Nature Physics* **8**, 819–824 (2012), doi:10.1038/nphys2423. URL `http://dx.doi.org/10.1038/nphys2423`.

10. H. Fan, S. Kumar, J. Sedlacek, H. Kübler, S. Karimkashi, and J. P. Shaffer, "Atom based RF electric field sensing," *J. Phys. B: At. Mol. Opt. Phys.* **48**(202001) (2015), doi:10.1088/0953-4075/48/20/202001. URL `https://doi.org/10.1088/0953-4075/48/20/202001`.

11. Y. Jiao, X. Han, Z. Yang, J. Li, G. Raithel, J. Zhao, and S. Jia, "Spectroscopy of cesium Rydberg atoms in strong radio-frequency fields," *Phys. Rev. A* **94**, 023832 (Aug 2016), doi:10.1103/PhysRevA.94.023832. URL `https://link.aps.org/doi/10.1103/PhysRevA.94.023832`.

12. S. A. Miller, D. A. Anderson, and G. Raithel, "Radio-frequency-modulated Rydberg states in a vapor cell," *New J. Phys.* **18**(053017) (2016), doi:10.1088/1367-2630/18/5/053017. URL `https://doi.org/10.1088/1367-2630/18/5/053017`.

13. C. L. Holloway, M. T. Simons, J. A. Gordon, A. Dienstfrey, D. Anderson, and G. Raithel, "Electric field metrology for SI traceability: Systematic measurement uncertainties in electromagnetically induced transparency in atomic vapor," *J. Applied Physics* **121**, 233106 (2017). URL `https://aip.scitation.org/doi/full/10.1063/1.4984201`.

14. D. A. Anderson, R. E. Sapiro, and G. Raithel, "Rydberg Atoms for Radio-Frequency Communications and Sensing: Atomic Receivers for Pulsed RF Field and Phase Detection," *IEEE Aerospace and Electronic Systems Magazine* **35**(4), 48–56 (2020), doi:10.1109/MAES.2019.2960922.

15. M. T. Simons, A. H. Haddab, J. A. Gordon, and C. L. Holloway, "A Rydberg atom-based mixer: Measuring the phase of a radio frequency wave," *Appl. Phys. Lett.* **114**, 114101 (2019), doi:10.1063/1.5088821.

16. J. A. Gordon, M. T. Simons, A. H. Haddab, and C. L. Holloway, "Weak electric-field detection with sub-1 Hz resolution at radio frequencies using a Rydberg atom-based mixer," *AIP Advances* **9**, 045030 (2019). URL `https://doi.org/10.1063/1.5095633`.

17. Y. Jiao, X. Han, J. Fan, G. Raithel, J. Zhao, and S. Jia, "Atom-based receiver for amplitude-modulated baseband signals in high-frequency radio communication," *Appl. Phys. Ex.* **12**, 126002 (2019), doi:10.7567/1882-0786/ab5463.

18. I. M. Savukov, S. J. Seltzer, and M. V. Romalis, "Tunable Atomic Magnetometer for Detection of Radio-Frequency Magnetic Fields," *Phys. Rev. Lett.* **95**, 063004 (2005), doi:10.1103/PhysRevLett.95.063004.

19. V. Gerginov, "Field-Polarization Sensitivity in rf Atomic Magnetometers," *Phys. Rev. Appl.* **11**, 024008 (2019), doi:10.1103/PhysRevApplied.11.024008.

20. V. Gerginov, F. C. S. da Silva, A. Hati, and C. Nelson, "An Atomic Sensor for Direct Detection of Weak Microwave Signals," *IEEE Trans. Microwave Theory Techniq.* **67**, 3485–3493 (2019), doi:10.1109/TMTT.2019.2921351.

21. V. Gerginov, F. C. S. da Silva, and D. Howe, "Prospects for magnetic field communications and location using quantum sensors," *Rev. Sci. Instrum.* **88**, 125005 (2017), doi:10.1063/1.5003821.

22. G. B. Chen, W. H. He, M. M. Dong, Y. Zhao, and G. X. Du, "Nitrogen-Vacancy Axis Orientation Measurement in Diamond Micro-Crystal for Tunable RF Vectorial Field Sensing," *IEEE Sens. J.* **20**, 2440–2445 (2020), doi:10.1109/JSEN.2019.2953359.

23. Y. Cohen, K. Jadeja, S. Sula, M. Venturelli, C. Deans, L. Marmugi, and F. Renzoni, "A cold atom radio-frequency magnetometer," *Appl. Phys. Lett.* **114**, 073505 (2019), doi:10.1063/1.5084004.

24. A. Terao, K. Ban, S. Ichihara, N. Mizutani, and T. Kobayashi, "Highly responsive ac scalar atomic magnetometer with long relaxation time," *Phys. Rev. A* **88**, 063413 (2013), doi:10.1103/PhysRevA.88.063413.

25. D. A. Keder, D. W. Prescott, A. W. Conovaloff, and K. L. Sauer, "An unshielded radio-frequency atomic magnetometer with sub-femtoTesla sensitivity," *AIP Adv.* **4**, 127159 (2014), doi:10.1063/1.4905449.

26. G. Bison, R. Wynands, and A. Weis, "Optimization and performance of an optical cardiomagnetometer," *J. Opt. Soc. Am. B* **22**, 77–87 (2005), doi:10.1364/JOSAB.22.000077.

27. M. Fleischhauer, A. Imamoglu, and J. P. Marangos, "Electromagnetically induced transparency: Optics in coherent media," *Rev. Mod. Phys.* **77**, 633–673 (Jul 2005), doi:10.1103/RevModPhys.77.633.

28. H. Shi, J. Ma, X. Li, J. Liu, C. Li, and S. Zhang, "A Quantum-Based Microwave Magnetic Field Sensor," *Sensors* **18**, 3288 (2018), doi:10.3390/s18103288.

29. F. Sun, D. Hou, Q. S. Bai, and X. H. Huang, "Rabi resonance in Cs atoms and its application to microwave magnetic field measurement," *J. Phys. Commun.* **2**(1), 015008 (2018), doi:10.1088/2399-6528/aaa11f.

30. A. Horsley and P. Treutlein, "Frequency-tunable microwave field detection in an atomic vapor cell," *Appl. Phys. Lett.* **108**, 211102 (2016), doi:10.1063/1.4950805.

31. P. Put, K. Popio lek, and S. Pustelny, "Different sensitivities of two optical magnetometers realized in the same experimental arrangement," *Sci. Rep.* **9**, 2537 (2019), doi:10.1038/s41598-019-39282-3.

32. R. J. Cooper, D. W. Prescott, G. J. Lee, and S. K. L., "RF atomic magnetometer array with over 40 dB interference suppression using electron spin resonance," *J. Magn. Reson.* **296**, 36–46 (2018), doi:10.1016/j.jmr.2018.08.007.

33. I. Savukov, S. Seltzer, and M. Romalis, "Detection of NMR signals with a radio-frequency atomic magnetometer," *J. Magn. Reson.* **185**, 214–220 (2007), doi:10.1016/j.jmr.2006.12.012.

34. N. Wilson, C. Perrella, R. Anderson, A. Luiten, and P. Light, "Wide-bandwidth atomic magnetometry via instantaneous-phase retrieval," *Phys. Rev. Res.* **2**(1), 013213 (2020), doi:10.1103/PhysRevResearch.2.013213.

35. S. Meiselman, G. Cranch, J. Lou, and S. Rittenhouse, "Rydberg Atom and Optically Excited Vapor Based RF Antennas," *NRL Memorandum Report* **NRL/5670/MR–2021/1** (2021).

36. N. Šibalić, J. D. Pritchard, C. S. Adams, and K. J. Weatherill, "Alkali Rydberg Calculator Python Library and Documentation," *GitHub* **Release 1.2** (2017). URL `https://github.com/nikolasibalic/ARC-Alkali-Rydberg-Calculator`.

37. A. Hurlock and M. N. Meiselman, S. Hutchinson, "Investigation of Multipass cells for Precision Electromagnetic Sensing," *NRL Memorandum Report* **NRL/MR/5675–19-9862** (2019).

38. Y. Xue, Y. Jiao, L. Hao, and J. Zhao, "Microwave two-photon spectroscopy of cesium Rydberg atoms," *Opt. Express* **29**(26), 43827–43835 (2021), doi:10.1364/OE.442703. URL `https://opg.optica.org/oe/abstract.cfm?URI=oe-29-26-43827`.

39. A. K. Robinson, N. Prajapati, D. Senic, and C. L. Simons, M. T.and Holloway, "Determining the angle-of-arrival of a radio-frequency source with a Rydberg atom-based sensor," *Appl. Phys. Lett.* **118**, 114001 (2021). URL `https://doi.org/10.1063/5.0045601`.

40. Sacher-Lasertechnik, "Caesium Spectroscopy - D2 Line," *Sacher-Lasertechnik GmbH* (2008). URL `https://www.sacher-laser.com/applications/overview/absorption_spectroscopy/caesium_d2.html`.

This page intentionally left blank

Appendix A

CATMIN 2022 POSTER

Below is copy of the poster presented by Dr. Rittenhouse at the Cold Atom Molecule Interactions (CATMIN) workshop, July 13-15, 2022 in Waterloo Canada, at the Perimeter Institute for Theoretical Physics. NRL/5670/PS–2022/1

133Cs as a low-frequency RF sensor

Seth T. Rittenhouse[1], Seth Meiselman[2], MIDN 1/C Vanessa Ortiz[1], and Geoffrey A. Cranch[2]

[1]*Department of Physics, The United States Naval Academy, Annapolis MD 21401, USA*
[2]*Optical Science Division, U. S. Naval Research Lab, Washington, DC 20375, USA*

U.S. NAVAL RESEARCH LABORATORY

Introduction

Due to their sensitivity to the external environment, Rydberg atoms make intriguing candidates for quantum mechanical sensors. Near-resonant RF fields with frequencies on the order of ~10 GHz can create measurable energy shifts in the spectrum with RF field amplitudes below $1\mu V/cm$ (see for instance [1-3]). However, at low frequencies (10 -100 MHz) the AC Stark sift tends to be fairly small for low amplitude fields making low intensity RF fields hard to sense. [4]

By using an offset DC field, the AC Stark spectrum becomes more sensitive to an additional low-amplitude RF field [5,6]. Here, we examine the sensitivity of the spectrum of Rydberg states of Cs (focusing on the 30s state) to a low amplitude, low frequency, RF field in the presence of a DC offset field. Employing Floquet theory, the energy and transition amplitude of the side band states are predicted. We find that the Rabbi frequency for transitions to these states from the $6P_{1/2}$ state is strongly dependent on the amplitude of the RF field. This sensitivity might be leveraged through EIT spectroscopy for low-frequency RF field detection.

Floquet and Sidebands

Schrödinger equation in the presence of a field with a periodic oscillation in the field:

$$i\hbar\frac{\partial|\Psi(t)\rangle}{\partial t} = \hat{H}(t)|\Psi(t)\rangle \qquad \hat{H}(t) = \sum_l e^{il\omega t}\hat{H}_l$$

Break into Fourier components:

$$|\Psi(t)\rangle = e^{-iEt/\hbar}\sum_m e^{-im\omega t}|\phi_m\rangle$$
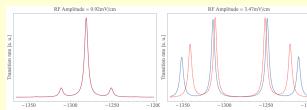
$$\sum_{m'}\hat{H}_{m'}|\phi_{m'-m}\rangle = (E + m\hbar\omega)|\phi_m\rangle$$

Coupling between Fourier components produces sidebands in the spectrum

Perturbation theory
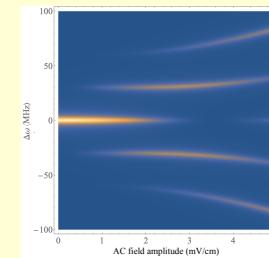
Energy and transition amplitude can be found perturbatively:

$$E_l = E_{DC} + l\hbar\omega \qquad \Omega_l \propto \left[J_l\left(\frac{\gamma F_{AC}}{\hbar\omega}\right)\right]^2$$
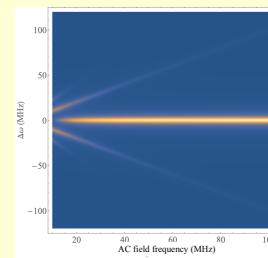
The predicted spectrum for transitions to the $30S_{1/2}$ state of ^{133}Cs in the presence of a 1 V/cm DC field with a 30 MHz RF field with a (small (left) and (right) larger (right) oscillation amplitude is shown. The blue solid curve is the full converged Floquet results, red dashed curve shows the result from

DC and AC Stark Shift

DC Stark spectrum of ^{133}Cs. Intensity is given by $30S_{1/2}$ admixture

slope γ determines sensitivity

Small fields produce a quadratic shift (as expected)

$$\Delta E_{DC} = \frac{1}{2}\alpha F^2$$

States from nearby nearly degenerate $27(\ell \geq 3)$ manifold create avoided crossings.

For weak, AC fields with slow oscillation, energy shift is give qualitatively by the time averaged DC shift

$$\Delta E_{AC} \sim \langle\Delta E_{DC}\rangle_t$$

Quadratic Stark effect means AC shift is fairly insensitive to small amplitude RF fields.

Solution: Use a DC offset to shift to a region in the Stark map with more sensitivity.

RF amplitude and Frequency Sensitivity
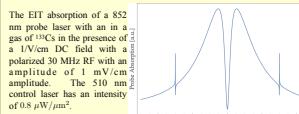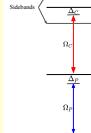
Spectrum for $30S_{1/2}$ state of ^{133}Cs in the presence of a 1 V/cm DC field with a 30 MHz RF field whose polarization matches the DC field. The spectrum is shifted to the DC Stark energy. There is a strong variation in sideband intensity with RF amplitude.

Spectrum for $30S_{1/2}$ state of ^{133}Cs is shown in the presence of a 1 V/cm DC field with a 1 mV/cm RF field whose polarization matches the DC field. Sidebands persist over a broad spectrum of RF frequencies.

EIT

Electromagnetically induced transparency provides an effective and efficient way to readout the position of the excited Rydberg states and the associated sideband states in the presence of an RF field.

The EIT absorption of a 852 nm probe laser with an in a gas of ^{133}Cs in the presence of a 1V/cm DC field with a polarized 30 MHz RF with an amplitude of 1 mV/cm amplitude. The 510 nm control laser has an intensity of 0.8 $\mu W/\mu m^2$.

(upper plot) The EIT spectrum when the control laser is resonant with the $6P_{1/2}$ to $30S_{1/2}$ transition and the probe detuning is swept through the $6S_{1/2}$ to $6P_{1/2}$ transition.

(lower plot) The probe laser is set to be resonant while the control laser frequency is swept through the resonance.

Multiple Frequencies

When several RF fields with incommensurate frequencies are combined, Floquet theory can still be applied:

$$|\Psi(t)\rangle = e^{-iE/\hbar}\sum_{\mathbf{m}} e^{-i\mathbf{m}\cdot\mathbf{\Omega}t}|\phi_{\mathbf{m}}\rangle$$

$$\mathbf{\Omega} = (\omega_1, \omega_2, ...) \quad \mathbf{m} = (m_1, m_2, ...)$$
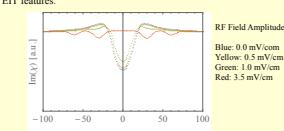
The Rydberg spectrum for 133Cs with a 1 V/cm offset fields and three RF fields of 30, 47, and 115 MHz is shown to the right as a function of the 115MHz field amplitude. The 30 and 47 MHz field amplitudes are set to 2 mV/cm.

Thermal Averaging

Because the two lasers have different frequencies, Doppler shift in counter-propagating lasers must be thermally averaged broadening the EIT features.

RF Field Amplitudes:
Blue: 0.0 mV/cm
Yellow: 0.5 mV/cm
Green: 1.0 mV/cm
Red: 3.5 mV/cm

The EIT absorption spectrum is shown for a room temperature (300 K) 133Cs gas in the presence of a 30 MHz RF field with a 1 V/cm DC offset as a function of control laser detuning frequency.

References

[1] J. A. Sedlacek, A. Schwettman, H. Kübler, R. Löw, T. Pfau, and J. P. Shaffer, Nature Physics 8, 819 (2012).
[2] D. A. Anderson, R. E Sapiro, and Georg Raithel, IEEE Aero. & Elec Sys. 35, 48-56 (2020).
[3] M.T Simmons, *et al.* App. Phys. Lett. 108, 174101 (2016).
[4] D. H. Meyer, *et al.*, J. of Phys. B, 53, 034001 (2020).
[5] Y.-Y. Jau and T. Carter, Phys. Rev. App. 13, 054034 (2020)
[6] L. Chai and R. Jones, 51st DAMOP, (2020) (http://meetings.aps.org/Meeting/ DAMOP20/Session/M02.2) Distribution A. Approved for public release, distribution is unlimited.

Fig. A1—Dist. A, Pub Release NRL/5670/PS–2022/1. A copy of the poster presented at CATMIN 2022

Appendix B

FOCAL SPOT SIZE

Both the pump and probe beams are needed to be collinear and counter-propagating within the atomic vapor cell. Additionally, to observe an EIT signal, and thereby verify creation of a Rydberg state, both beams need to achieve appropriate intensities. For comparison we scaled our experimental parameters to align with values from [16, 38, 39]. The probe beam is focused to a smaller spot size and Rayleigh range than that of the pump beam to ensure that the probe response is only from atoms effected by the pump. From these calculations, as shown in Fig. B1 and Fig. B2, very little laser power is required from both beams to achieve corresponding intensities from the references, and thus an EIT resonance, in the small interaction volume of our experimental setup.

The working setup has a 510 nm Rayleigh range of 20 cm, with a focal spot diameter of 180 microns. The 852 nm Rayleigh range is 3.2 cm, with a focal spot diameter of 93 microns. The ratio of intensities of the probe to pump beam is about 4E-3.

The following code was written to assist summer intern MIDN Ortiz with appropriate placement of planoconvex lenses to observe EIT in room temperature cesium vapor:

```
%
% Coded for Matlab by Seth Meiselman and Vanessa Ortiz, June 2022
% Calculation of focal spot size, Rayleigh range,
% and intensity of Rydberg pump and probe
%

clear all;
lambda = 0.512526; % microns  - our choice - wavelength
D = 1.9:0.05:2.1; % mm - starting diameter of beam
F1 = 100; % mm - FIXED - focal point of lens 1
F2 = 100; % mm - FIXED - focal point of lens 2
d = 207:0.01:220; % mm - variable - distance between lenses

for i = 1:size(d,2)
  % mm - calculated out - total focal point of two lenses
    F(i) = 1/( (1/F1)+(1/F2)-(d(i)/(F1*F2)) );
    for j = 1:size(D,2)
  % microns - calculated out - diameter of focus
        wo(i,j) = (2*lambda/pi)*(F(i)/D(j));
% mm - calculated out - Rayleigh range
        ZR(i,j) = (10^-3)*pi*(wo(i,j)^2)/lambda;
    end
end

area510 =(wo.^2).*pi; %microns ^2
pow510 = 2.25; %mW
intensity510 = 1000*pow510./area510; %1000*nW/(m^2) or 1000*mW/um^2 or uW/mm^2


fig1 = figure(1);
set(fig1,'Name', '510 calculations',...
'units','normalized','Position', [0.02 0.1 0.45 0.7])
subplot(2,2,1);
```

```
%figure(3); %distance between lenses, total focal point
plot(d,F); xlabel('distance between lenses(mm)');
ylabel('510 total focal point distance(mm)');
 xlim([min(d) max(d)]);
%figure(1); %starting diameter of beam, distance between lenses, diameter of focus
subplot(2,2,2);
s = surf(D(:),d(:),wo(:,:)); view(2); colorbar, caxis([-400 -80]);
 s.EdgeColor = 'none'; ylabel('distance between lenses(mm)');
xlabel('starting beam diameter(mm)');
 title('510 beam waist(microns)'); axis([min(D) max(D) min(d) max(d)]);
%figure(2); %starting diameter of beam, distance between lenses, Rayleigh range
subplot(2,2,3);
a = surf(D(:),d(:),ZR(:,:)); view(2); colorbar; caxis([50 600]);
 a.EdgeColor = 'none'; ylabel('distance between lenses(mm)');
xlabel('starting beam diameter(mm)');
 title('510 Rayleigh range(mm)'); axis([min(D) max(D) min(d) max(d)]);
%figure(7);
subplot(2,2,4);
s = surf(D(:),d(:),intensity510(:,:)); view(2); colorbar%, caxis([0.0001 0.001]);
 s.EdgeColor = 'none'; xlabel('starting beam diameter(mm)');
ylabel('distance between lenses(mm)');
 title('510 intensity(uW/mm^2)'); axis([min(D) max(D) min(d) max(d)]);

lambda2 = 0.85233557; % microns  - our choice
D2 = 1.9:0.05:2.1; % mm - ???
F12 = 100; % mm - FIXED
F22 = 100; % mm - FIXED
d2 = 207:0.01:235; % mm - variable

for i = 1:size(d2,2)
    F2(i) = 1/( (1/F12)+(1/F22)-(d2(i)/(F12*F22)) ); % mm - calculated out
    for j = 1:size(D2,2)
        wo2(i,j) = (2*lambda2/pi)*(F2(i)/D2(j)); % microns - calculated out
        ZR2(i,j) = (10^-3)*pi*(wo2(i,j)^2)/lambda2; % mm - calculated out
    end
end

area852 =(wo2.^2).*pi; %microns ^2
pow852 = .0023; %mW
intensity852 = 1000*pow852./area852; %1000*nW/(m^2) or 1000*mW/um^2 or uW/mm^2

fig4 = figure(4);
set(fig4,'Name', '852 calculations',...
'units','normalized','Position', [0.5 0.1 0.45 0.7])
%figure(6);
subplot(2,2,1);
plot(d2,F2); xlabel('distance between lenses(mm)');
ylabel('total focal point distance(mm)');
 xlim([min(d2) max(d2)]);
subplot(2,2,2);
%figure(4);
s2 = surf(D2(:),d2(:),wo2(:,:)); view(2); colorbar; caxis([-400 -80]);
 s2.EdgeColor = 'none'; ylabel('distance between lenses(mm)');
xlabel('starting beam diameter(mm)');
 title('852 beam waist(microns)'); axis([min(D2) max(D2) min(d2) max(d2)]);
%figure(5);
subplot(2,2,3);
 a2 = surf(D2(:),d2(:),ZR2(:,:)); view(2); colorbar; caxis([50 600]);
 a2.EdgeColor = 'none'; ylabel('distance between lenses(mm)');
xlabel('starting beam diameter(mm)');
 title('852 Rayleigh range(mm)'); axis([min(D2) max(D2) min(d2) max(d2)]);
%figure(8);
subplot(2,2,4);
s = surf(D2(:),d2(:),intensity852(:,:)); view(2); colorbar%, caxis([0.0001 0.001]);
 s.EdgeColor = 'none'; xlabel('starting beam diameter(mm)');
ylabel('distance between lenses(mm)');
```

```
 title('852 intensity(uW/mm^2)'); axis([min(D2) max(D2) min(d2) max(d2)]);

% 852 and 510 from DOI 10.1063/1.5095633
A =[49 60600]; % uW 34D 5/2
r = [425 620]/2; % um
I = A./(pi*r.^2);

% 852 and 510 from DOI 10.1063/5.0045601
A =[96 60000]; % uW 59S 1/2
r = [390 450]/2; % um
I = A./(pi*r.^2);

% 852 and 510 from DOI 10.1364/OE.442703
OMG =[17.2 4.4]; % MHz, OMG/2PI 68D 5/2
r = [90 135]/2; % um
I = A./(pi*r.^2);

% their 852 and 510 unknown DOI
A =[360 40000]; % uW
r = [330 390]/2; % um
I = A./(pi*r.^2);

% our 852 and 510
A =[2.3 2250]; % uW
r = [93 180]/2; % um
I = A./(pi*r.^2);

% EOF
```
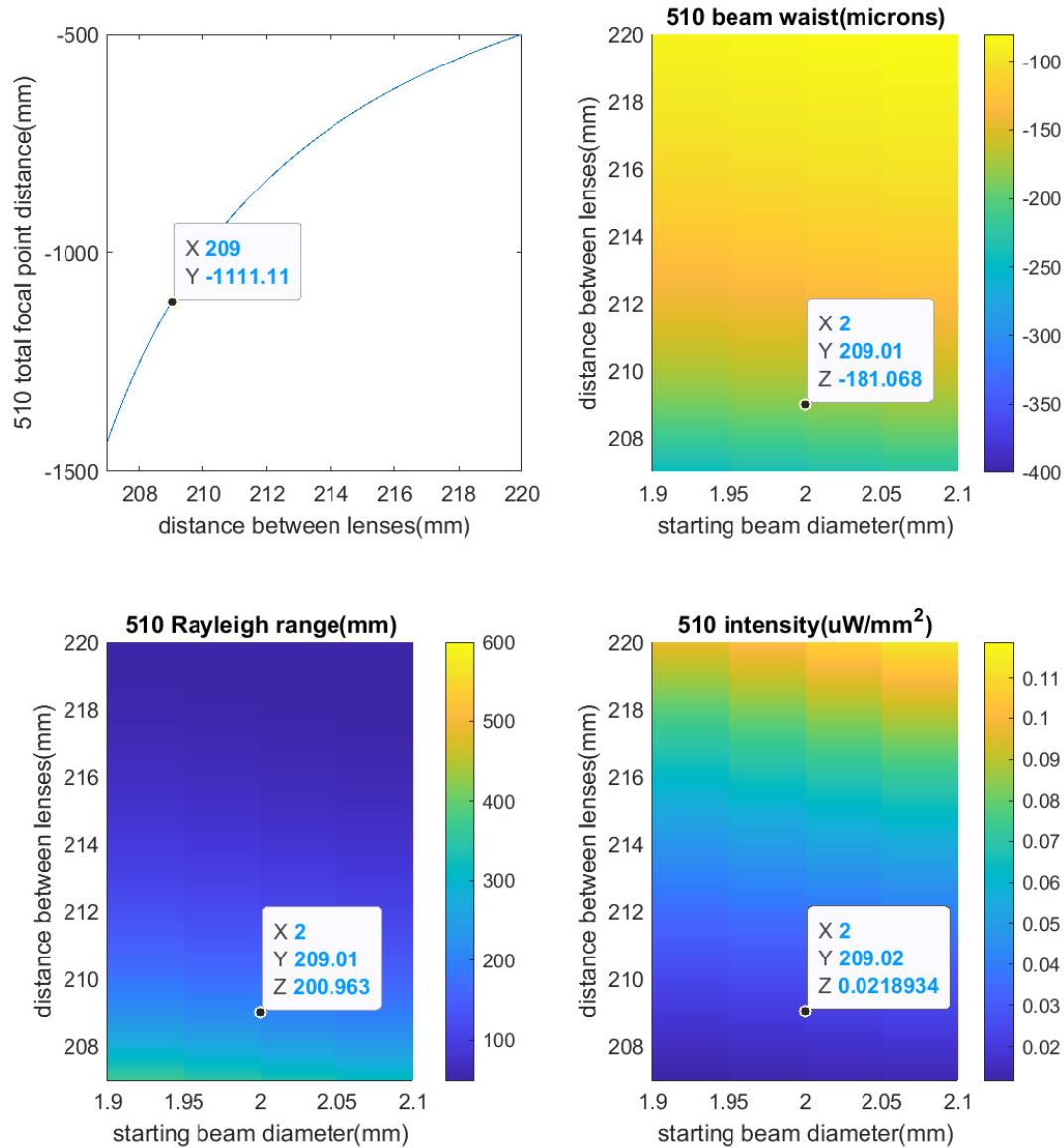
Fig. B1—Calculation output from Matlab code used to appropriately space planoconvex lenses to create the required 510 nm laser intensity. The calculation also yields the Rayleigh range and position relative to the lenses.
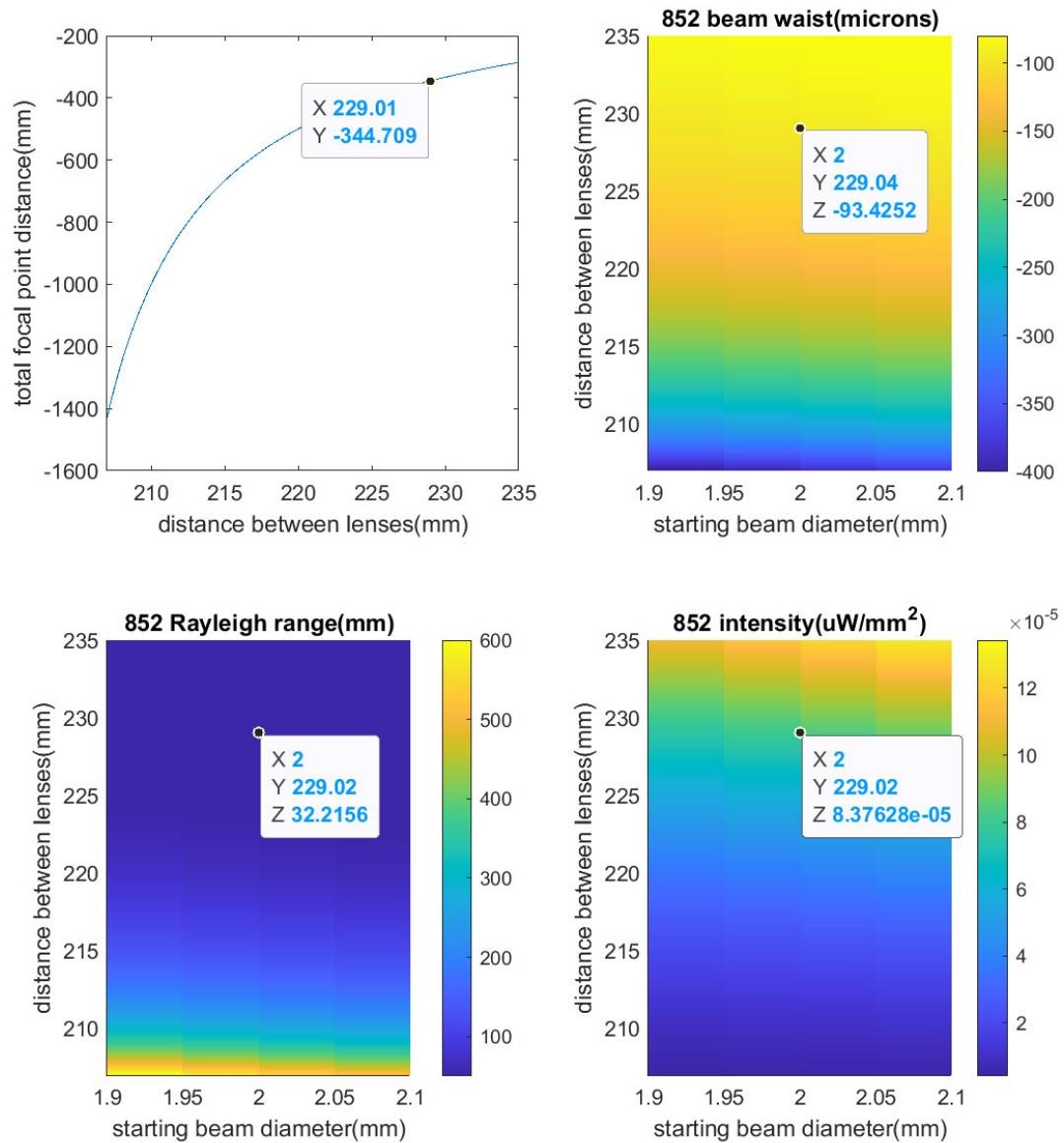
Fig. B2—Calculation output from Matlab code used to appropriately space planoconvex lenses to create the required 510 nm laser intensity. The calculation also yields the Rayleigh range and position relative to the lenses.

This page intentionally left blank

Appendix C

ABSORPTION COEFFICIENTS

The following code was written and amended to guide standard light-atom interaction parameter identification. Fig. C1 shows the relative vapor pressure of alkali (earth) species with respect to changes in ambient temperature. This directly relates to both average number density and thermal velocities of the atoms and in turn can be used to estimate interaction numbers, for both overall strength and fundamental resolution, and transit time broadening. Fig. C2 displays colormaps of room temperature cesium vapor absorption and reflection coefficients for the ground state transition with 852 nm light. Fig. C3 shows estimates for Doppler, power, and self-broadening effects on the total decay rate from the D1 and D2 lines in room temperature cesium vapor. Information from the previous appendix could be used to modify this code to further generate other broadening mechanisms of interest such as transit time broadening into a single calculator script.

```
%%%%%%%%%%%%%%%%%%%%%%%%%%%%%%%%%%%%%%%%%%%%%%%%%%%%%%%%%%%%%%%%%%%%%%%%%
%   Version 2   -   Absorption Lengths of the Alkali Vapors
%                -   including density vs. temperature and linewidths
%
%  Converted for Matlab by Seth Meiselman, 2017-08-18, edit 2020-01-03
%  Original coding in Mathematica by Virginia Lorenz, version 3/9/2010
%
% v1: Initial values are those taken from Lorenz code.
% Other 'filler' values added for complete execution for all
% alkali species.
% v2: Structures and cells were implemented to neaten the workspace.
% Plots are created with respect to monitor size, the native
% resolution was 1900x1200 on a ~20"x13" monitor, rescaling may be
% necessary for other dimensions. Breaking figures up into species is
% also straight forward by adusting the figure window lines -- 153,
% 690, 727, and 828 -- and putting them into the for loop that
% follows.
%
% Structures:
%  Though not explicitly required, the code is written in a
%  top-down fashion where functions are created and called when
%  needed.
% Functions are contained in the cv. structure.
% Constants are contained in the const. structure.
% Alkali data are within the alkali. structure.
% Absorption, reflection, index and epsilon are in absp.
%
% Part 1.0
%  1.a Definition of natural constants
% Part 2.0
% 2.a Clear namespace of pressure curve constants and functions
%  2.b Define pressure curve constants for each species
%  2.c Define pressure conversion functions
%  2.d Define functions of pressure, density, and velocity
%  2.e Plotting of pressure, density, and velocity of all species
%  2.f Unused - secondary definitions
%  2.g Calc. single wavelength blackbody radiation amplitude
%  2.h Calc. Argon buffer gas equivalent pressure
% Part 3.0
%  3.a Clear and define En, nu, and lambda conversion functions
%  3.b Unused - alkali species data
```

```
%   3.c Define alkali species data for broadening
%   3.d Define broadening mechanisms: doppler, power, collisional
%   3.e Plotting decay rates vs temperature
%   3.f Plotting shifts and splittings vs temperature
%  Part 4.0
%   4.a Define epsilon, ref. index, abs., refl., and 1/e depth
%   4.b Plot abs. refl. and 1/e depth
%  Part 5.0 End of file
%
% v3: Future goals:
% Check all alkali data values with accepted literature results
%  Extend low n state calculation to high n(<100) for Rydberg levels
%  this should significantly increase the computation time, limit
%  output to single species.
% types of collisional broadening
%  blackbody AC Stark shift and broadening for Rydberg states
% mechanism for potential ionization
% time of flight/ interaction window limitation
% finally, include Stark effect on high n levels
%
%%%%%%%%%%%%%%%%%%%%%%%%%%%%%%%%%%%%%%%%%%%%%%%%%%%%%%%%%%%%%%%%%%%%%%%%%%
clear; close all; tic; toc % empty memory, code runtime
%% Part 1.0 Constants of nature: setup
for zz = 1:1

%% Part 1.a Constants of nature: definitions
    clear const.kB const.NA amu h const.hbar c const.Names const.ccgs const.ecgs const.mcgs;
      const.kB = 1.38064852/1E23; % [J/K]     Boltzmann's constant
      const.NA = 6.02214086*1E23; % [1/mol]   Avagadro's number
     const.amu = 1.66053904/1E27; % [kg]      unified atomic mass unit
       const.e = 1.60217653/1E19; % [C]       electron's charge
       const.h = 6.62607004/1E34; % [Js]      Planck's constant
    const.hbar = const.h/(2*pi); % [Js]       reduced Planck's const 1.0545718/1E34
       const.c = 299792458; % [m/s]     speed of light in vacuum
      const.me = 9.1093826/1E31; % [kg]       electron's mass
    const.eps0 = 8.854187817/1E12; % [F/m]     permittivity of free space
     const.cer = (const.e^2)/(4*pi*const.eps0*const.me*const.c^2); % [m]    classical electron radius
      const.a0 = 0.52917720859/1E10;% [m] Bohr radialkali.US

    const.ccgs = 2.99792458*1E10; % [cm/s]    c in cgs units
    const.ecgs = 4.803/1E10; % [esu]     e in cgs units
    const.mcgs = 9.1093826/1E28; % [g]        me in cgs units
    const.rcgs = (const.ecgs^2)/(const.mcgs*const.ccgs^2); % [cm]  const.cer in cgs units

%   atom     1   2   3   4   5   6     used as indexing term later
    const.Names = ['Li';'Na';'K ';'Rb';'Cs';'Ba']; % used set of species const.Names

% const.xx structure includes the natural constants, as seen above and
% other single use constants as described in various steps below
end

%% Part 2.0 Calculating vapor pressure, density, and thermal velocity for atomic species
for zz = 1:1

%% Part 2.a Clear variable namespace
    for z = 1:1
% constants in log(p) = A+B/T+CT+Dlog10(T)
        clear pcurve.Aa pcurve.Bb pcurve.Cc pcurve.Dd ...
            alkali.matom;           % see Gehm 2003, Properties of Lithium 6
                        % as liquids? or as solids?
        clear cv.Nn ...    % density function of temperature
            cv.P ...      % pressure function of temperature
            cv.u ...      % velocity function of temperature
            cv.Ncgs ... % '' in cgs units
            T;          % temperature variable
        %   pressure is in Torr or mmHg
```

```
    %    temperature is in celcialkali.US for some eqns
    %                and kelvin in others?
    %    density N is in 1/m^3
    %    density Ncgs in in 1/cm^3 (cgs units)
    clear alkali.TS alkali.NS alkali.US alkali.PS alkali.NScgs;    % arrays for plotting
    clear Tlist Plist Nlist Nlistcm Nlistcgs ulist; % arrays for plotting
end

%% Part 2.b Species properties: definitions
% pressure equation constants, mass(amu) melting temp(K)
    for z = 1:1
    % Lithium
            pcurve.Aa(1) = 12.9992;
            pcurve.Bb(1) = -8442.53;
            pcurve.Cc(1) = 2.5968/1E4;
            pcurve.Dd(1) = -1.64038*log10(10);
        alkali.matom(1) = 6.941;    % amu
        alkali.tmelt(1) = 453.7;    % kelvin
    % Sodium
            pcurve.Aa(2) = 2.881+4.704;
            pcurve.Bb(2) = -5377;
            pcurve.Cc(2) = 0;
            pcurve.Dd(2) = 0;
        alkali.matom(2) = 22.9897692807;   % amu
        alkali.tmelt(2) = 370.9;           % kelvin
    % Potassium
            pcurve.Aa(3) = 13.83624;
            pcurve.Bb(3) = -4857.902;
            pcurve.Cc(3) = 0.0003494;
            pcurve.Dd(3) = -2.212542;
        alkali.matom(3) = 39.0983; % amu
        alkali.tmelt(3) = 336.6;    % kelvin
    % Rubidium
            pcurve.Aa(4) = 2.881+4.312;
            pcurve.Bb(4) = -4040;
            pcurve.Cc(4) = 0;
            pcurve.Dd(4) = 0;
        alkali.matom(4) = 0.5*(84.912+86.909); % amu
        alkali.tmelt(4) = 312.45;              % kelvin
    % Cesium
            pcurve.Aa(5) = 8.22127;
            pcurve.Bb(5) = -4006.048;
            pcurve.Cc(5) = -0.00060194;
            pcurve.Dd(5) = -0.19623;
            alkali.matom(5) = 132.905451931;    % amu
            alkali.tmelt(5) = 301.6;            % kelvin
    % Barium
            pcurve.Aa(6) = 6.99;
            pcurve.Bb(6) = -8980;
            pcurve.Cc(6) = -0;
            pcurve.Dd(6) = -0;
        alkali.matom(6) = 137.33;  % amu
        alkali.tmelt(6) = 1000;    % kelvin

        alkali.matomkg = alkali.matom/(const.NA*1000);
    end

%% Part 2.c Pressure conversion functions
    for z = 1:1
        cv.mmHg2atm = @(mmHg) mmHg/760;
        cv.mmHg2Pa = @(mmHg) (mmHg/760)*(1.01E5);
                % or 133.322368 or 400/3, alkali.USed below
        cv.mmHg2lbin = @(mmHg) 14.7*mmHg/760;
        cv.atm2mmHg = @(atm) 760*atm;
    end
```

```
%% Part 2.d Functions for pressure P, density N, and velocity u
for z = 1:1
cv.P = @(atom,T) 10^( pcurve.Aa(atom) +pcurve.Bb(atom)/T +pcurve.Cc(atom)*T +pcurve.Dd(atom)*log10(T)/log10(10) );
cv.Nn = @(atom,T) cv.P(atom,T+273)*4*100/(3*const.kB*(T+273));
cv.Ncgs = @(atom,T) cv.Nn(atom, T)/1E6;
cv.u = @(atom, T) sqrt((8*const.kB*(T+273))/(pi*alkali.matomkg(atom)))/1000;
for atom = 1:6
for i = 1:150
%% Part 2.d.1 Definition of TS(atom,:) alkali.USed later for temperature vector
% TS and NS are alkali.USed later for simplifying & shorter runtime
alkali.TS(atom,i) = 5*i; % temperature in Celsius
alkali.PS(atom,i) = cv.P(atom,alkali.TS(atom,i)+273); % pressure in mmHg or Torr abs temp in Kelvin
alkali.NS(atom,i) = cv.Nn(atom,alkali.TS(atom,i)); % density in 1/m^3 temp input in Celsius
alkali.NScgs(atom,i) = alkali.NS(atom,i)./1E6; % density in 1/cm^3 temp input in Celsius
alkali.US(atom,i) = cv.u(atom,alkali.TS(atom,i)); % speed in m/s temp input in Celsius
end
end
end

%% Part 2.e Plotting of pressure, density, and velocity
% single figure output: three subplots
% subplot 1: P vs T for all atom species
% subplot 2: N vs T for all atom species
% subplot 3: u vs T for all atom species
for z = 1:1
fig1 = figure(1);
set(fig1,'Name', 'Pressure, Density, Avg. Velocity',...
'units','normalized','Position', [0.025 0.15 0.2 0.7])
for atom = 1:6
subplot(3,1,1);
semilogy(alkali.TS(atom,:),alkali.PS(atom,:), 'DisplayName', const.Names(atom,:));
title('Vapor Pressure'); xlabel('T [^{o}C]'); ylabel('P [Torr]');
hold on;

subplot(3,1,2);
semilogy(alkali.TS(atom,:),alkali.NS(atom,:), 'DisplayName', const.Names(atom,:));
title('Number Density'); xlabel('T [^{o}C]'); ylabel('N [1/m^{3}]');
hold on;

subplot(3,1,3);
plot(alkali.TS(atom,:),alkali.US(atom,:), 'DisplayName', const.Names(atom,:));
title('Avg. Velocity'); xlabel('T [^{o}C]'); ylabel('u [nm/ps]');
hold on;
end
subplot(3,1,1); axis tight; hold off; legend('show');
subplot(3,1,2); axis tight; hold off; legend('show');
subplot(3,1,3); axis tight; hold off; legend('show');
end

%% Part 2.f Unalkali.USed - Second array of pressure, density, and velocity, etc.
    for z = 1:1
%        for atom = 1:6
%            for i = 1:30
%                Tlist(atom,i) = 60*i;
%                Plist(atom,i) = P(atom,TS(atom,i)+273);
%                Nlist(atom,i) = Nn(atom,TS(atom,i));
%                ulist(atom,i) = u(atom,Tlist(atom,i));
%                %Nlistcm(atom,i) = Nn(atom,TS(atom,i))/1E6;
%                Nlistcgs(atom,i) = NS(atom,i)./1E6;
%            end
%        end
    end

%% Part 2.g Simplified calculation of blackbody radiation
% calc. single wavelength BBR photon count at specific temp
for z = 1:1
```

```
const.Tbb = 800+273;      %   blackbody temperature in kelvin
const.lambb = 554/1E9;    %   wavelength in m
const.nubb = const.c/const.lambb;    %   freq. in Hz
% Planck's Law
const.IntPlanck = ((2*const.h*const.nubb^3)/(const.c^3))*(1/(exp((const.h*const.nubb)/(const.kB*const.Tbb))-1));
% is the emitted power per unit area of emitting surface
% in the normal direction, per unit solid angle [W/sr/m^2]
% energy per photon
const.Enbb = const.h*const.c/const.lambb;
% photons per second
const.phps = 4*pi*const.IntPlanck/const.Enbb;
end


%% Part 2.h Argon pressure equal to barium pressure at varioalkali.US temperatures
% calc loading number density from loading temperature and
% pressure, then calc new pressure given fixed particle
% number and new work temperature
for z = 1:1
clear T Tset;
cv.Pideal = @(atom,T,Tset) (const.kB*(T+273)*cv.Nn(atom,Tset))/((4*100)/(3));
const.Tload = 27;
for atom = 1:6
for i = 1:150
pcurve.TsetList(atom,i) = 5*i;
pcurve.Tset(atom) = pcurve.TsetList(atom,i);
pcurve.PidealList(atom,i) = cv.Pideal(atom,const.Tload+273,pcurve.TsetList(atom,i));
pcurve.PidealListatm(atom,i) = cv.mmHg2atm(pcurve.PidealList(atom,i));
end
end
const.Pargon = 0.003395108857112331; % this value seems sketchy where does it come from
const.NArgon = (4*100*const.Pargon)/(3*const.kB*(27+273));
%        fprintf( strcat('   Density of Argon for \n    Pargon = ',...
%                         num2str(Pargon),...
%                         ' [Torr] \n    loaded at Temp = ',...
%                         num2str(const.Tload), ...
%                         ' [C] \n   is const.NArgon =',...
%                         num2str(const.NArgon),' [1/m^3]\n') );
const.Tsetpoint = 700;
const.PArT700=(const.kB*(const.Tsetpoint+273)*const.NArgon)/((4*100)/3);
%        fprintf( strcat('   Pressure of Argon at Temp = ',...
%                         num2str(Tsetpoint), ...
%                         ' [C] for \n    Pargon = ',...
%                         num2str(Pargon),...
%                         ' [Torr] loaded at const.Tload = ',...
%                         num2str(const.Tload),...
%                         ' [C] \n   is Pargon(700) =',...
%                         num2str(PArT700),' [1/m^3]\n') );
% pressure of argon vs temp
clear PArg;
const.PArg0 = 400;
const.NArg0 = ((400/3)*const.PArg0)/(const.kB*(const.Tload+273));
cv.PArg = @(T) (const.kB*(T+273)*const.NArg0)/(400/3);
cv.PArg(1000);
end


end


%% Part 3.0 Linewidth setup
for zz = 1:1


%% Part 3.a Clear/define conversion function namespace
for z = 1:1
clear lam dlam omg omgcgs nu dnu En dEn; % conversion between
clear cv.lam2nu cv.dlam2dnu cv.lam2En cv.dlam2dEn; % wavelength,
clear cv.nu2lam cv.dnu2dlam cv.nu2En cv.dnu2dEn; % energy,
clear cv.En2lam cv.dEn2dlam cv.En2nu cv.dEn2dnu; % and frequency
```

```
  cv.omg = @(lam) 2*pi*const.c/lam;
    cv.lam2nu = @(lam) const.c/lam;
 cv.dlam2dnu = @(lam, dlam) (-const.c/lam^2)*dlam;
    cv.lam2En = @(lam) (const.h/const.e)*cv.lam2nu(lam);
 cv.dlam2dEn = @(lam, dlam) (const.h/const.e)*cv.dlam2dnu(lam, dlam);
    cv.nu2lam = @(nu) const.c/nu;
 cv.dnu2dlam = @(nu, dnu) (-const.c/nu^2)*dnu;
     cv.nu2En = @(nu) (const.h*nu/const.e);
  cv.dnu2dEn = @(dnu) (const.h*dnu/const.e);
     cv.En2nu = @(En) (const.e/const.h)*En;
  cv.dEn2dnu = @(dEn) (const.e/const.h)*dEn;
    cv.En2lam = @(En) -const.c/cv.En2nu(En);
 cv.dEn2dlam = @(En, dEn) (-const.c/cv.En2nu(En)^2)*cv.dEn2dnu(dEn);
 end

%% Part 3.b Unalkali.USed - Species transitions calculations
for z = 1:1
% Li 2S --> 3P
lam(1,1) = 670.8/1E9;
nu0(1,1) = const.c/lam(1,1);
lamtot(1) = 323/1E9;
nutot(1) = const.c/lamtot(1);
nu0(1,2) = nutot(1) - nu0(1,1);
lam(1,2) = const.c/nu0(1,2);
% const.NA
lam(2,1) = 589/1E9;
nu0(2,1) = const.c/lam(2,1);
lamtot(2) = 342.8/1E9;
nutot(2) = const.c/lamtot(2);
nu0(2,2) = nutot(2) - nu0(2,1);
lam(2,2) = const.c/nu0(2,2);
% K 4^2S_{1/2} --> 5^2P_{5/2}
lam(3,1) = 767/1E9;
nu0(3,1) = const.c/lam(3,1);
lamtot(3) = 404.4/1E9;
nutot(3) = const.c/lamtot(3);
nu0(3,2) = nutot(3) - nu0(3,1);
lam(3,2) = const.c/nu0(3,2);
% Rb 5^2S_{1/2} --> 5^2P_{3/2}
lam(4,1) = 780/1E9;
lam(4,2) = 775.8/1E9;
nu0(4,1) = const.c/lam(4,1);
nu0(4,2) = const.c/lam(4,2);
lamtot(4) = const.c/(nu0(4,1)+nu0(4,2));
% Rb 5^2S_{1/2} --> 6^2P_{3/2} --> 5^2P_{3/2}
lam(4,3) = 420.2/1E9;
lam(4,4) = 389/1E9;
nu0(4,3) = const.c/lam(4,3);
nutot(4) = const.c/lam(4,4);
lamtot(4) = const.c/(nutot(4) - nu0(4,3));
% Cs 6^2S_{1/2} --> 8S_{1/2}
lam(5,1) = 852/1E9;
lamtot(5) = 411/1E9;
nu0(5,1) = const.c/lam(5,1);
nutot(5) = const.c/lamtot(5);
nu0(5,2) = nutot(5) - nu0(5,1);
lam(5,2) = const.c/nu0(5,2);
% Cs 6^2S_{1/2} --> 7P_{1/2} --> 8S_{1/2}
lam(5,3) = 460/1E9;
nu0(5,3) = const.c/lam(5,3);
lam(5,4) = const.c/(nutot(5) - nu0(5,3));
% Ba 6s^2^1S_{0} --> 6s6p^1P_{1}
lam(6,1) = 553.5/1E9;
nu0(6,1) = const.c/lam(6,1);
nutot(6) = nu0(6,1);
```

```
lamtot(6) = const.c/(nutot(6) - nu0(6,1));
% Number of atoms in beam of 1 micron diameter
%((10^18)^(2/3))*(10^-8); % ????

clear lam nu0 nutot lamtot;
end

%% Part 3.c Species data input
% from AIP Physics Desk Reference combined with Maki, J. J.
% and Malcuit, M. S. and Sipe, J. E. and Boyd, R. W., "Linear and
% Nonlinear Optical Measurements of the Lorentz Local Field," Phys. Rev.
% Lett. 67, 8 (1991).
for z = 1:1
% Lithium ---- empty/bogalkali.US entries
for zzz = 1:1
% transition wavelengths
% D Lines
alkali.lam0(1,1) = 100/1E9; % m
alkali.lam0cgs(1,1) = alkali.lam0(1,1)*10^2; % cm
alkali.lam0(1,2) = 200/1E9; % m
alkali.lam0cgs(1,2) = alkali.lam0(1,2)*10^2; % cm
% oscillator strengths
% from Correlation effects in a relativistic calculation of the
% 6s2 S01-6s6p P13,1P1 transitions in barium, J.Migdalek and
% W.E.Baylis, 1987*)
alkali.f(1,1) = 1; % from http://www.nist.gov/srd/upload/jpcrd614.pdf
alkali.f(1,2) = 2; % from http://www.nist.gov/srd/upload/jpcrd614.pdf
% weights
alkali.g(1,10) = 1;
alkali.g(1,1) = 1;
alkali.g(1,2) = 2;
% const.NAtural decay rates
alkali.ynat(1,1) = 1*10^8; % Hz
alkali.ynat(1,2) = 2*10^8; % Hz
% dipole moments
alkali.d(1,1) = 1/1E29; % C m
alkali.d(1,2) = 2/1E29; % C m
% atomic mass
alkali.Mamu(1) = 6; % amu
alkali.M(1) = alkali.Mamu(1)*const.amu; % kg

% collisioconst.NAl shift coefficients (from Maki)
alkali.C6(6) = 0.64/1E77;
alkali.C12(6) = 0.76/1E133;

alkali.beta(6,1) = -(5./1E14);
alkali.betacgs(6,1) = -(5./1E8);
end

% Sodium
for zzz = 1:1
% transition wavelengths
% D Lines
alkali.lam0(2,1) = 589.5924/1E9; % m
alkali.lam0(2,2) = 588.9950/1E9; % m
alkali.lam0cgs(2,1) = alkali.lam0(2,1)*10^2; % cm
alkali.lam0cgs(2,2) = alkali.lam0(2,2)*10^2; % cm
% 3P --> 3D Transition
alkali.lam0(2,3) = 819.4824/1E9; % m
alkali.lam0(2,4) = 818.3256/1E9; % m
alkali.lam0cgs(2,3) = alkali.lam0(2,3)*10^2; % cm
alkali.lam0cgs(2,4) = alkali.lam0(2,4)*10^2; % cm
% oscillator strengths
alkali.f(2,1) = 0.614;
alkali.f(2,2) = 0.616;
alkali.f(2,3) = 0.54;
```

```
alkali.f(2,4) = 0.453;
% weights
alkali.g(2,10) = 2;
alkali.g(2,1) = 2;
alkali.g(2,2) = 4;
alkali.g(2,3) = 4;
alkali.g(2,4) = 4;
% const.NAtural decay rates
alkali.ynat(2,1) = 0.6135379*10^8; % Hz
alkali.ynat(2,2) = 0.6154229*10^8;
alkali.ynat(2,3) = 1/(19/1E9);
alkali.ynat(2,4) = 1/(19/1E9); % check
% dipole moments
alkali.d(2,1) = 2.492323*const.e*const.a0; % C m
alkali.d(2,2) = 3.5246*const.e*const.a0;
alkali.d(2,3) = 0.537*const.e*const.a0; % check
% atomic mass
alkali.Mamu(2) = 22.989769280728; % amu
alkali.M(2) = alkali.Mamu(2)*const.amu; % kg

% collisioconst.NAl shift coefficients (from Maki)
alkali.C6(2) = 0.64/1E77;
alkali.C12(2) = 0.76/1E133;

alkali.beta(2,1) = -(5./1E14);
alkali.beta(2,2) = -(3./1E14);
alkali.betacgs(2,1) = -(5./1E8);
alkali.betacgs(2,2) = -(3./1E8);
end

% Potassium
for zzz = 1:1
% transition wavelengths
% D Lines
alkali.lam0(3,1) = 769.89645/1E9; % m
alkali.lam0(3,2) = 766.48991/1E9; % m
alkali.lam0cgs(3,1) = alkali.lam0(3,1)*10^2; % cm
alkali.lam0cgs(3,2) = alkali.lam0(3,2)*10^2; % cm
% 4P_{3/2} --> 4D Transition
alkali.lam0(3,3) = 693.6/1E9; % m
alkali.lam0cgs(3,3) = alkali.lam0(2,3)*10^2; % cm
% oscillator strengths
alkali.f(3,1) = 0.339463548;
alkali.f(3,2) = 0.6817342151;
alkali.f(3,3) = 0.1; % check
% weights
alkali.g(3,10) = 2;
alkali.g(3,1) = 2;
alkali.g(3,2) = 4;
alkali.g(3,3) = 2; % check
% const.NAtural decay rates
alkali.ynat(3,1) = 0.382*10^8; % Hz
alkali.ynat(3,2) = 0.387*10^8;
alkali.ynat(3,3) = 1/(500/1E9);
% dipole moments
alkali.d(3,1) = 1.6/1E29; % C m
alkali.d(3,2) = 1.6591834/1E29;
alkali.d(3,3) = 0.537*const.e*const.a0; % check
% atomic mass
alkali.Mamu(3) = 39.0983; % amu
alkali.M(3) = alkali.Mamu(3)*const.amu; % kg

% collisioconst.NAl shift coefficients (from Maki)
alkali.C6(3) = 0.64/1E77;
alkali.C12(3) = 0.76/1E133;
```

```
alkali.beta(3,1) = -(5./1E14);
alkali.beta(3,2) = -(3./1E14);
alkali.betacgs(3,1) = -(5./1E8);
alkali.betacgs(3,2) = -(3./1E8);
end

% Rubidium
for zzz = 1:1
% transition wavelengths
% D Lines
alkali.lam0(4,1) = 794.97901493396/1E9; % m
alkali.lam0(4,2) = 780.24136827127/1E9; % m
alkali.lam0cgs(4,1) = alkali.lam0(4,1)*10^2; % cm
alkali.lam0cgs(4,2) = alkali.lam0(4,2)*10^2; % cm
% 5P_{3/2} --> 5D_{5/2} Transition
alkali.lam0(4,3) = 776/1E9; % m
alkali.lam0cgs(4,3) = alkali.lam0(4,3)*10^2; % cm
% oscillator strengths
alkali.f(4,1) = 0.3423197;
alkali.f(4,2) = 0.6957729;
alkali.f(4,3) = 0.003*alkali.f(4,2); % check
% weights
alkali.g(4,10) = 2;
alkali.g(4,1) = 2;
alkali.g(4,2) = 4;
alkali.g(4,3) = 6;
% const.NAtural decay rates
alkali.ynat(4,1) = 0.3612936*10^8; % Hz
alkali.ynat(4,2) = 0.3811711*10^8;
alkali.ynat(4,3) = 1/(235/1E9);
% dipole moments
alkali.d(4,1) = 2.993120*const.e*const.a0; % C m
alkali.d(4,2) = 4.2275287*const.e*const.a0;
alkali.d(4,3) = sqrt(300/90000)*4.2275287*const.e*const.a0; % check
% atomic mass
alkali.Mamu(4) = 84.91178973214; % amu
alkali.M(4) = alkali.Mamu(4)*const.amu; % kg

% collisioconst.NAl shift coefficients (from Maki)
alkali.C6(4) = 0.64/1E77;
alkali.C12(4) = 0.76/1E133;

alkali.beta(4,1) = -(5./1E14);
alkali.beta(4,2) = -(3./1E14);
alkali.betacgs(4,1) = -(5./1E8);
alkali.betacgs(4,2) = -(3./1E8);
end

% Cesium
for zzz = 1:1
% transition wavelengths
% D Lines
alkali.lam0(5,1) = 894.59295986/1E9; % m
alkali.lam0(5,2) = 852.34727582/1E9; % m
alkali.lam0cgs(5,1) = alkali.lam0(5,1)*10^2; % cm
alkali.lam0cgs(5,2) = alkali.lam0(5,2)*10^2; % cm
% 6P_{3/2} --> 8S_{1/2} Transition
alkali.lam0(5,3) = 818.5/1E9; % m
alkali.lam0cgs(5,3) = alkali.lam0(5,3)*10^2; % cm
% oscillator strengths
alkali.f(5,1) = 0.3438;
alkali.f(5,2) = 0.7148;
alkali.f(5,3) = 0.1; % ?? check
% weights
alkali.g(5,10) = 2;
alkali.g(5,1) = 2;
```

```
alkali.g(5,2) = 4;
alkali.g(5,3) = 2; % check
% const.NAtural decay rates
alkali.ynat(5,1) = 0.34894*10^8; % Hz
alkali.ynat(5,2) = 0.32815*10^8;
alkali.ynat(5,3) = 1/(155/1E9);
% dipole moments
alkali.d(5,1) = 2.6980/1E29; % C m
alkali.d(5,2) = 3.7971/1E29;
alkali.d(5,3) = 0.537*const.e*const.a0; % check
% atomic mass
alkali.Mamu(5) = 132.905451931; % amu
alkali.M(5) = alkali.Mamu(5)*const.amu; % kg

% collisioconst.NAl shift coefficients (from Maki)
alkali.C6(5) = 0.64/1E77;
alkali.C12(5) = 0.76/1E133;

alkali.beta(5,1) = -(5./1E14);
alkali.beta(5,2) = -(3./1E14);
alkali.betacgs(5,1) = -(5./1E8);
alkali.betacgs(5,2) = -(3./1E8);
end


% Barium
for zzz = 1:1
% transition wavelengths
% D Lines
alkali.lam0(6,1) = 553.5/1E9; % m
alkali.lam0cgs(6,1) = alkali.lam0(6,1)*10^2; % cm
alkali.lam0(6,2) = 100/1E9; % m
alkali.lam0cgs(6,2) = alkali.lam0(6,2)*10^2; % cm
% oscillator strengths
% from Correlation effects in a relativistic calculation of the
% 6s2 S01-6s6p P13,1P1 transitions in barium, J.Migdalek and
% W.E.Baylis, 1987*)
alkali.f(6,1) = 1.64; % from http://www.nist.gov/srd/upload/jpcrd614.pdf
alkali.f(6,2) = 2; % from http://www.nist.gov/srd/upload/jpcrd614.pdf
% weights
alkali.g(6,10) = 1;
alkali.g(6,1) = 3;
alkali.g(6,2) = 2;
% const.NAtural decay rates
alkali.ynat(6,1) = 0.6135379*10^8; % Hz
alkali.ynat(6,2) = 2*10^8; % Hz
% dipole moments
alkali.d(6,1) = 1.5257/1E29; % C m
alkali.d(6,2) = 2/1E29; % C m
% atomic mass
alkali.Mamu(6) = 137.327; % amu
alkali.M(6) = alkali.Mamu(6)*const.amu; % kg

% collisioconst.NAl shift coefficients (from Maki)
alkali.C6(6) = 0.64/1E77;
alkali.C12(6) = 0.76/1E133;

alkali.beta(6,1) = -(5./1E14);
alkali.beta(6,2) = -(3./1E14);
alkali.betacgs(6,1) = -(5./1E8);
alkali.betacgs(6,2) = -(3./1E8);
end

end

%% Part 3.d Broadening characteristics and calculations
for zzz = 1:1
```

```
%% Part 3.d.1 Foreign Gas
for z = 1:1
const.Mfor = 20.18; % amu ???
alkali.Mred(:) = (alkali.M(:)*const.Mfor)./(alkali.M(:)+const.Mfor);
const.Pfor = 200; % loaded pressure
const.Nfor = (4*100*const.Pfor)/(3*(const.kB*(27+273)));
const.mforkg = const.Mfor/(const.NA*1000);
cv.vfor = @(T) sqrt((8*const.kB*(T+273))/(pi*const.mforkg));
end

%% Part 3.d.2 Broadening mechanisms
% unused function?
cv.eta = @(rho,atom,T) ((63*pi*alkali.C12(atom))/(256*const.hbar*cv.vfor(T)*(rho^11)))-...
((3*pi*alkali.C6(atom))/(8*const.hbar*cv.vfor(T)*(rho^5)));
% FWHM for 4*pi*N for v for int_{0}^{infty}{(1 - \cos(eta[\rho]))*\rho*d\rho}

% laser parameters
const.Ilaser = 6E8; % W/m^2 % corresponds to ~0.5 mW avg power

% broadening mechanisms
for z = 1:1
clear nu0 omg0 En0 dlam domg y i lam dnucol dnuL yself ytot T lmin lmax;
for atom = 1:6
for i = 1:2
% frequencies
alkali.nu0(atom,i) = const.c/alkali.lam0(atom,i); % Hz
alkali.omg0(atom,i) = 2*pi*alkali.nu0(atom,i); % rad/s
% energies
alkali.En0(atom,i) = cv.nu2En(alkali.nu0(atom,i)); % eV
end % i loop
end % atom loop

% doppler broadening
% dlamdoppler = @(atom, i, T) (3.58/1E7)*lam0(atom,i)*...
% sqrt((T+273)/M(atom)); % m
cv.dlamdop = @(atom, i) (7.16/1E7)*alkali.lam0(atom,i).*...
sqrt((alkali.TS(atom,:)+273)/alkali.Mamu(atom)); % m
cv.ydop = @(atom, i) (const.c/alkali.lam0(atom,i)^2).*...
cv.dlamdop(atom,i); % 1/s
% resoconst.NAnce (self) broadening
cv.yres = @(atom, i) alkali.f(atom,i)*const.cer*alkali.lam0(atom,i)*...
const.c*((alkali.g(atom,10)/alkali.g(atom,i))^(1/2))*...
alkali.NS(atom,:); % 1/s
% foreign gas broadening
const.yfor = ones(1,size(alkali.TS,2))*const.Pfor*8E7; % ??????
% power broadening
cv.ypow = @(atom, i) ones(1,size(alkali.TS,2))*alkali.ynat(atom,i)*... % 1/s
sqrt(1+(2*const.Ilaser*alkali.d(atom,i)^2)/(const.hbar* alkali.ynat(atom,i))^2);
% collisioconst.NAl shift
cv.dnucol = @(atom, i) alkali.beta(atom,i)*alkali.NS(atom,:);
cv.dlamcol = @(atom, i) cv.dnu2dlam(alkali.nu0(atom,i),cv.dnucol(atom,i));
cv.dEncol = @(atom, i, T) cv.dnu2dEn(cv.dnucol(atom,i));
% Lorentz-Lorenz shift
cv.dnuL = @(atom, i) (-1/3)*alkali.f(atom,i)*const.cer*alkali.lam0(atom,i)*...
const.c*alkali.NS(atom,:);
cv.dlamL = @(atom, i) cv.dnu2dlam(alkali.nu0(atom,i),cv.dnuL(atom, i));
cv.dEnL = @(atom, i) cv.dnu2dEn(cv.dnuL(atom, i));
% total decay rate
cv.ytot = @(atom,i) (1/2)*alkali.ynat(atom,i)*ones(1,size(alkali.TS,2))+...
cv.ydop(atom,i) +...
cv.yres(atom,i) +...
const.yfor + cv.ypow(atom,i); % 1/s
% shifted resoconst.NAnces
cv.lam0shift = @(atom,i) alkali.lam0(atom,i)*ones(1,size(alkali.TS,2)) + cv.dlamcol(atom,i) + ...
cv.dlamL(atom,i);
```

```
cv.nu0shift = @(atom,i) alkali.nu0(atom,i)*ones(1,size(alkali.TS,2)) + cv.dnucol(atom,i) + ...
cv.dnuL(atom,i);
cv.En0shift = @(atom,i) alkali.En0(atom,i)*ones(1,size(alkali.TS,2)) + cv.dEncol(atom,i) + ...
cv.dEnL(atom,i);

cv.lamsplit = @(atom) (alkali.lam0(atom,2) - alkali.lam0(atom,1))*ones(1,size(alkali.TS,2));
cv.nusplit = @(atom) (alkali.nu0(atom,2) - alkali.nu0(atom,1))*ones(1,size(alkali.TS,2));
cv.Ensplit = @(atom) (alkali.En0(atom,2) - alkali.En0(atom,1))*ones(1,size(alkali.TS,2));
cv.lamsplitshift = @(atom) cv.lam0shift(atom,2) - cv.lam0shift(atom,1);
cv.nusplitshift = @(atom) cv.nu0shift(atom,2) - cv.nu0shift(atom,1);
cv.Ensplitshift = @(atom) cv.En0shift(atom,2) - cv.En0shift(atom,1);


end

const.Tmin = 25;
const.Tmax = 700;
const.Tset = 600;
const.T = const.Tset;

% calculate arrays of decay rates vs temperature --- currently unused
for atom = 1:6
%  ydop1(atom,:) = ydop(atom,1);
%  yres1(atom,:) = yres(atom,1);
%  ypow1(atom,:) = ypow(atom,1);
%
%  ydop2(atom,:) = ydop(atom,2);
%  yres2(atom,:) = yres(atom,2);
%  ypow2(atom,:) = ypow(atom,2);
%
%   ytot1(atom,:) = ytot(atom,1);
%  ytot2(atom,:) = ytot(atom,2);
end
end

%% Part 3.e Plotting of decay rates vs temperature
for zzz = 1:1
fig10 = figure(10);
set(fig10,'Name', 'Decay Rates',...
'units','normalized','Position', [0.005 0.15 0.9 0.7]);
for atom = 1:6
x1 = 0.05+(atom-1)*0.16;
pos1 = [x1 0.1 0.14 0.55];
pos2 = [x1 0.65 0.14 0.3];
%  subplot(3,6,[atom (atom+6)]);
subplot('Position', pos1);
semilogy(alkali.TS(atom,:),cv.ydop(atom,1),'DisplayName', strcat(const.Names(atom,:),': |1> doppler'));
hold on;
semilogy(alkali.TS(atom,:),cv.yres(atom,1),'DisplayName', strcat(const.Names(atom,:),': |1> resoconst.NAnce'));
semilogy(alkali.TS(atom,:),cv.ypow(atom,1),'DisplayName', strcat(const.Names(atom,:),': |1> power'));
semilogy(alkali.TS(atom,:),cv.ydop(atom,2),'DisplayName', strcat(const.Names(atom,:),': |2> doppler'));
semilogy(alkali.TS(atom,:),cv.yres(atom,2),'DisplayName', strcat(const.Names(atom,:),': |2> resoconst.NAnce'));
semilogy(alkali.TS(atom,:),cv.ypow(atom,2),'DisplayName', strcat(const.Names(atom,:),': |2> power'));
semilogy(alkali.TS(atom,:),const.yfor,'DisplayName', 'foreign gas');
axis tight; legend('show', 'location', 'southeast');
title('Decay Rates'); xlabel('T [^{o}C]');if atom == 1, ylabel('\gamma [1/s]'); end
hold off;

%  subplot(3,6,(atom+12));
subplot('Position', pos2);
semilogy(alkali.TS(atom,:),cv.ytot(atom,1),'DisplayName', strcat(const.Names(atom,:),': |1> total'));
hold on;
semilogy(alkali.TS(atom,:),cv.ytot(atom,2),'DisplayName', strcat(const.Names(atom,:),': |2> total'));
axis tight; legend('show', 'location', 'northwest');
title('Decay Rates'); xlabel('T [^{o}C]'); if atom ==1, ylabel('\gamma [1/s]');end
hold off;
```

```
end

% % print block of
% %  constants name level splitting data chart
% % level splitting w/ shifts state values
% % is missing setup for execution
end

%% Part 3.f Plotting of shifts and splittings vs temperature
for zzz = 1:1
fig20 = figure(20);
set(fig20,'Name', 'Decay Rates',...
'units','normalized','Position', [0.005 0.15 0.9 0.7]);
for atom = 1:6
%   x1 = 0.05+(atom-1)*0.16;
%   pos1 = [x1 0.1 0.14 0.55];
%   pos2 = [x1 0.65 0.14 0.3];
subplot(6,6,atom);
%  subplot('Position', pos1);
plot(alkali.TS(atom,:),cv.lam0shift(atom,1),'DisplayName', '|1> shift');
hold on;
plot(alkali.TS(atom,:),cv.lam0shift(atom,2),'DisplayName', '|2> shift');
axis tight; legend('show', 'location', 'southwest'); title(const.Names(atom,:));
if atom == 1, ylabel('\lambda(T) [m]'); end %xlabel('T [^{o}C]');
hold off;
subplot(6,6,(atom+6));
%  subplot('Position', pos1);
plot(alkali.TS(atom,:),cv.nu0shift(atom,1),'DisplayName', '|1> shift');
hold on;
plot(alkali.TS(atom,:),cv.nu0shift(atom,2),'DisplayName', '|2> shift');
axis tight; legend('show', 'location', 'southwest');
if atom == 1, ylabel('\nu(T) [Hz]'); end %xlabel('T [^{o}C]');
hold off;
subplot(6,6,(atom+12));
%  subplot('Position', pos1);
plot(alkali.TS(atom,:),cv.En0shift(atom,1),'DisplayName', '|1> shift');
hold on;
plot(alkali.TS(atom,:),cv.En0shift(atom,2),'DisplayName', '|2> shift');
axis tight; legend('show', 'location', 'southwest');
if atom == 1, ylabel('En(T) [eV]'); end %xlabel('T [^{o}C]');
hold off;

subplot(6,6,(atom+18));
%  subplot('Position', pos2);
plot(alkali.TS(atom,:),cv.lamsplit(atom),'DisplayName', 'before');
hold on;
plot(alkali.TS(atom,:),cv.lamsplitshift(atom),'DisplayName', 'shifted');
axis tight; legend('show', 'location', 'northwest');
if atom ==1, ylabel('\Delta\lambda(T)');end %xlabel('T [^{o}C]');
hold off;
subplot(6,6,(atom+24));
%  subplot('Position', pos2);
plot(alkali.TS(atom,:),cv.nusplit(atom),'DisplayName', 'before');
hold on;
plot(alkali.TS(atom,:),cv.nusplitshift(atom),'DisplayName', 'shifted');
axis tight; legend('show', 'location', 'northwest');
if atom ==1, ylabel('\Delta\nu(T)');end %xlabel('T [^{o}C]');
hold off;
subplot(6,6,(atom+30));
%  subplot('Position', pos2);
plot(alkali.TS(atom,:),cv.Ensplit(atom),'DisplayName', 'before');
hold on;
plot(alkali.TS(atom,:),cv.Ensplitshift(atom),'DisplayName', 'shifted');
axis tight; legend('show', 'location', 'northwest');
if atom ==1, ylabel('\Delta En(T)');end %xlabel('T [^{o}C]');
hold off;
```

```
end
clear pos1 pos2 x1;

end

end

%% Part 4.0 Absorption Coefficient
for zz = 1:1

%% Part 4.a Calculation of permitivity, refractive index,
% absorption, reflectance, and 1/e depth
for z = 1:1
for i =1:2
cv.epspart{i} = @(atom, lam) ((4*pi*alkali.NS(atom,:)*alkali.f(atom,i)*...
const.cer*alkali.lam0(atom,i))/(const.eps0*const.c)).*...
((1)./(alkali.omg0(atom,i)*ones(1,size(alkali.TS,2))-...
cv.omg(lam)*ones(1,size(alkali.TS,2))-1i*cv.ytot(atom,i))+...
(1)./(alkali.omg0(atom,i)*ones(1,size(alkali.TS,2))+...
cv.omg(lam)*ones(1,size(alkali.TS,2))+1i*cv.ytot(atom,i)));
end
cv.epsilon = @(atom,lam) 1 + cv.epspart{1}(atom,lam) + cv.epspart{2}(atom,lam);
cv.index = @(atom,lam) sqrt(cv.epsilon(atom,lam));
cv.alpha = @(atom,lam) (4*pi*imag(cv.index(atom,lam)))/(lam);
cv.reflc = @(atom, lam) ((cv.index(atom,lam)-1)./(cv.index(atom,lam)+1)).*...
conj((cv.index(atom,lam)-1)./(cv.index(atom,lam)+1));
cv.depth = @(atom,lam) (1)./(cv.alpha(atom,lam));

% limits are set for states 1 and 2
cv.lmin = @(atom) (min(alkali.lam0(atom,1:2))*1E9 - 10)/1E9;
cv.lmax = @(atom) (max(alkali.lam0(atom,1:2))*1E9 + 10)/1E9;
cv.lstep = @(atom) (cv.lmax(atom)-cv.lmin(atom))/(size(alkali.TS,2)-1);

for atom = 1:6
for i = 1: size(alkali.TS,2)
absp.index{atom}(i,:) = cv.index(atom,(cv.lmin(atom)+cv.lstep(atom)*i));
absp.alpha{atom}(i,:) = cv.alpha(atom,(cv.lmin(atom)+cv.lstep(atom)*i));
absp.reflc{atom}(i,:) = cv.reflc(atom,(cv.lmin(atom)+cv.lstep(atom)*i));
absp.depth{atom}(i,:) = cv.depth(atom,(cv.lmin(atom)+cv.lstep(atom)*i));
end
end
end

%% Part 4.b Surface plotting of abs, refl, depth vs temperature, wavelength
for z = 1:1
fig30 = figure(30);
set(fig30,'Name', 'Absorption',...
'units','normalized','Position', [0.005 0.15 0.9 0.7]);
for atom = 1:6
x1 = 0.05+(atom-1)*0.16;
x2 = 0.171+(atom-1)*0.16;
pos1 = [x1 0.08 0.12 0.22];
pos2 = [x1 0.40 0.12 0.22];
pos3 = [x1 0.72 0.12 0.22];

subplot('Position', pos3);
%    subplot(3,6,atom);
surf(alkali.TS(atom,:),cv.lmin(atom):cv.lstep(atom):cv.lmax(atom),absp.alpha{atom}); view(2); shading interp;
axis tight; title(strcat(const.Names(atom,:),': Abs. coeff. [1/m]'));  colormap jet;
cbar = colorbar;
cbar.Position(3) = 0.2*cbar.Position(3);
cbar.Position(1) = x2;
ylabel('\lambda [m]'); xlabel('T [^{o}C]');

subplot('Position', pos2);
%  subplot(3,6,(atom+6));
```

```
surf(alkali.TS(atom,:),cv.lmin(atom):cv.lstep(atom):cv.lmax(atom),absp.reflc{atom}); view(2); shading interp;
axis tight; title(strcat(const.Names(atom,:),': Refl. coeff. [a.u]'));  colormap jet;
cbar = colorbar;
cbar.Position(3) = 0.2*cbar.Position(3);
cbar.Position(1) = x2;
ylabel('\lambda [m]'); xlabel('T [^{o}C]');

subplot('Position', pos1);
%  subplot(3,6,(atom+12));
surf(alkali.TS(atom,:),cv.lmin(atom):cv.lstep(atom):cv.lmax(atom),absp.depth{atom}); view(2); shading interp;
axis tight; title(strcat(const.Names(atom,:),': 1/e Depth [m]'));  colormap jet;
cbar = colorbar;
cbar.Position(3) = 0.2*cbar.Position(3);
cbar.Position(1) = x2;
ylabel('\lambda [m]'); xlabel('T [^{o}C]');

end
clear pos1 pos2 pos3 x1 x2 cbar;
end
clear fig1 fig10 fig20 fig30 atom;

end


%% Part 5.0 End of File, clean up
clear i z zz zzz ans;
toc % code runtime
% EOF
```
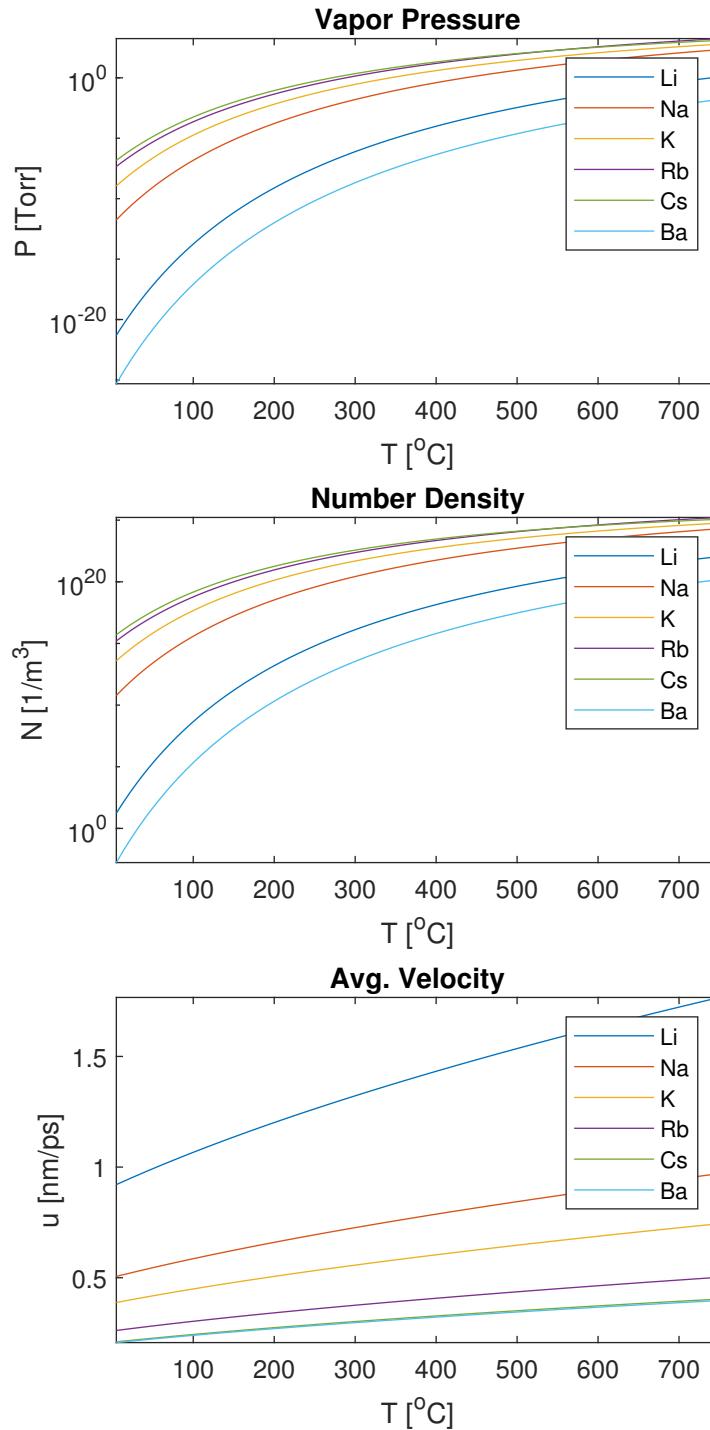
Fig. C1—Numerical calculation of atomic species (Li, Na, K, Rb, Cs, and Ba) vapor pressure, number density, and average (thermal) velocity with respect to temperature.
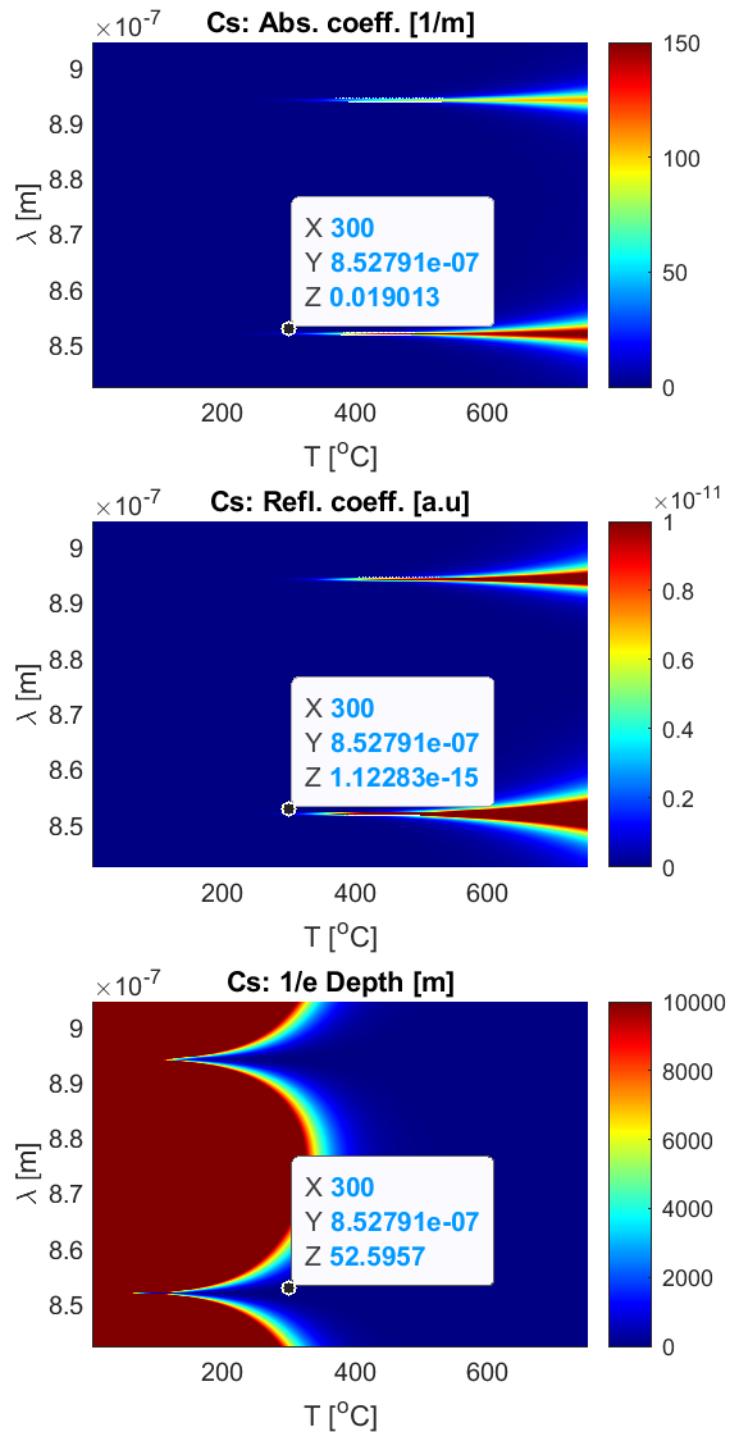
Fig. C2—Numerical calculation of the ground state transition absorption and reflection coefficients.
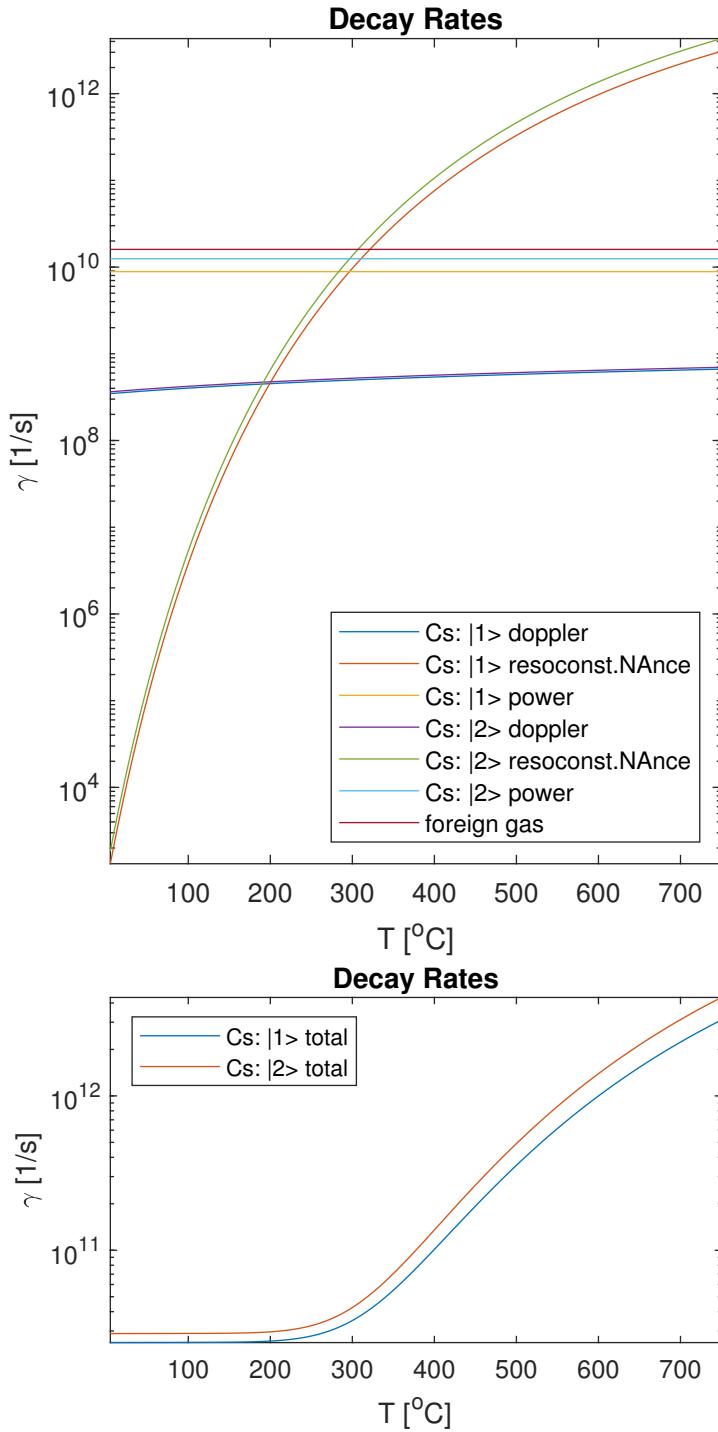
Fig. C3—Numerical calculation of the ground state transition's approximate decay rates due to various mechanisms dependent on operating temperature: Doppler, power, foreign gas, and self-broadening.

Appendix D

MISC. REFERENCE MATERIAL
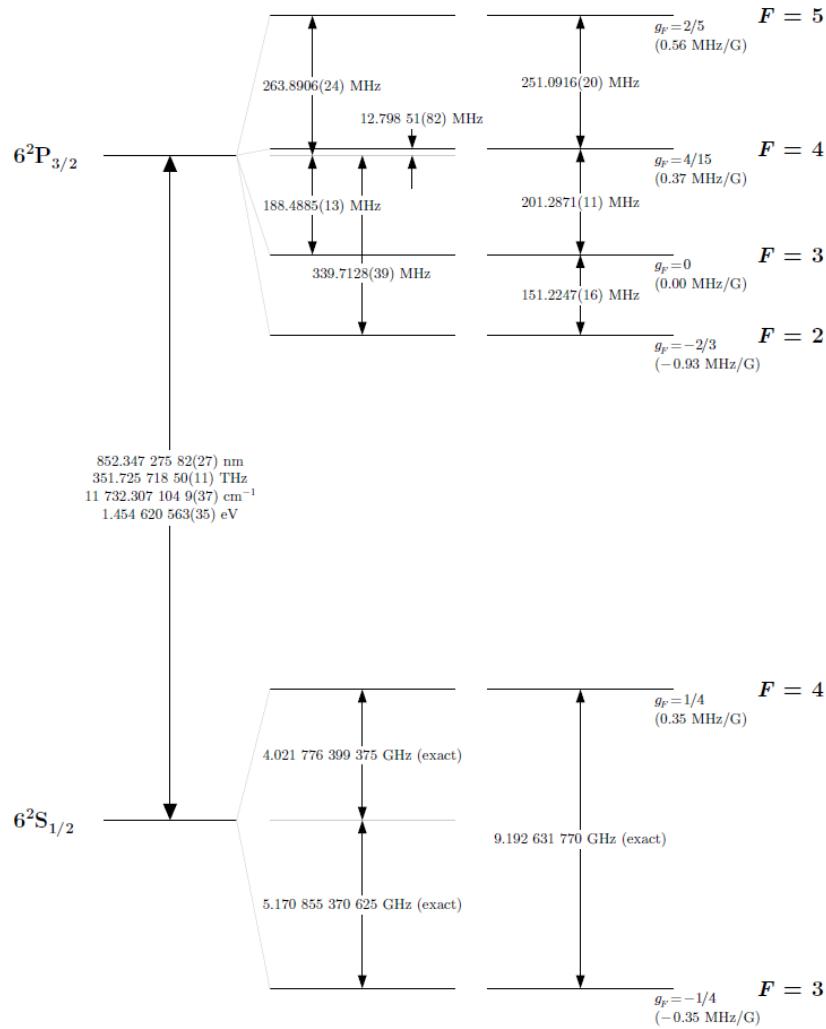
Figure 2: Cesium D$_2$ transition hyperfine structure, with frequency splittings between the hyperfine energy levels. The excited-state values are taken from [30], and the ground-state values are exact, as a result of the current definition of the second. The relative hyperfine shifts are shown to scale within each hyperfine manifold (but visual spacings should not be compared between manifolds or to the optical splitting). The approximate Landé g_F-factors for each level are also given, with the corresponding Zeeman splittings between adjacent magnetic sublevels.

Fig. D1—Figure and original caption from [?], Cesium D2 line energy diagram.
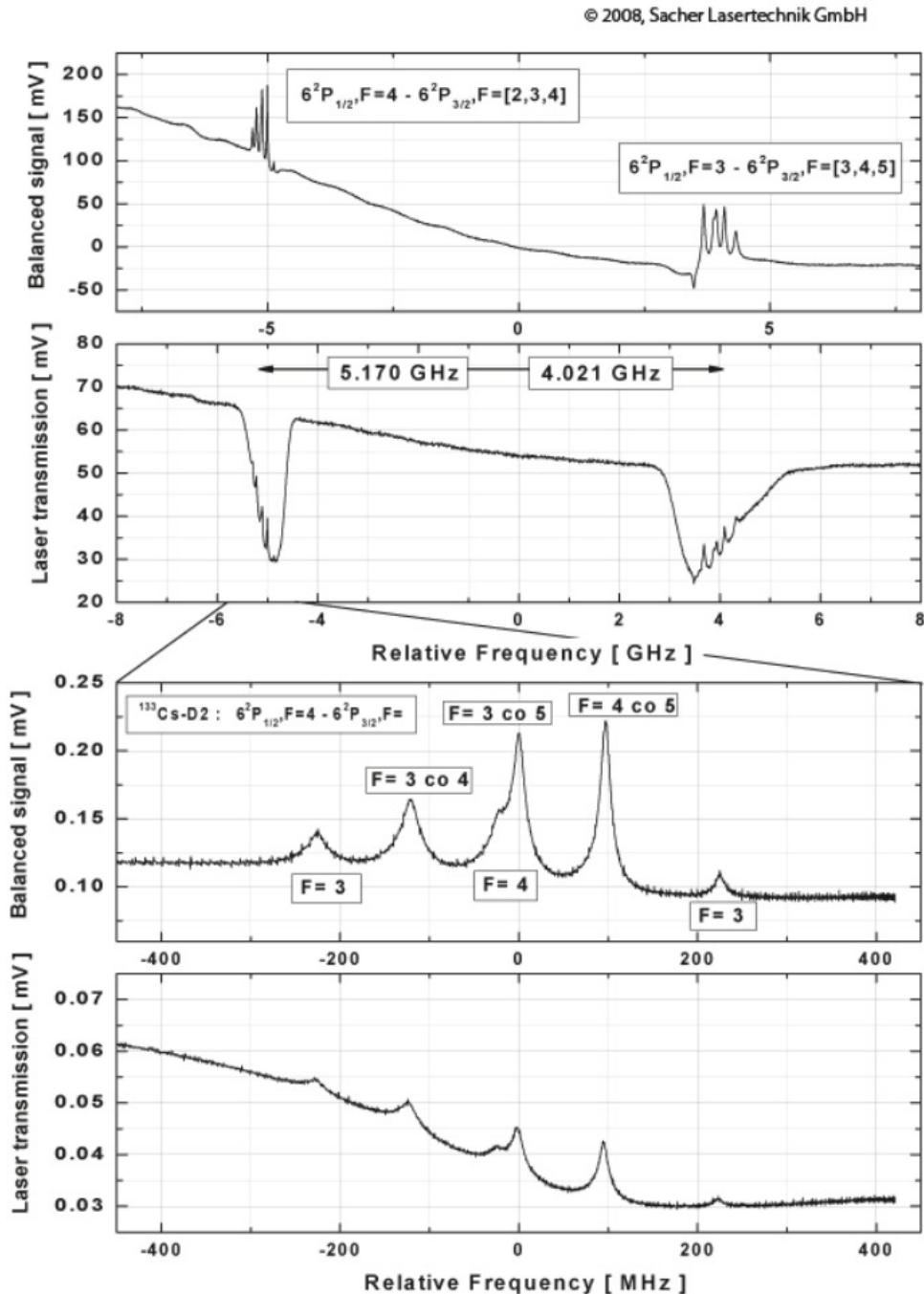
Fig. D2—The spectra show the saturated absorption of the D2 line of Cesium at 852nm.
[40]